

**Investigation of Deep Levels  
in Monocrystalline  $\text{CuInSe}_2$**

by

A. L. Li

A thesis submitted to the Faculty of Graduate Studies  
and Research in partial fulfilment of the requirements  
for the degree of Master of Engineering

Department of Electrical Engineering  
McGill University  
Montreal, Canada  
July, 1991

**To the Memory of My Grandmother**

## Abstract

Homojunctions of  $\text{CuInSe}_2$  were fabricated by diffusing indium or bismuth into monocrystalline substrates grown by a vertical Bridgman method. The current-voltage characteristics at different temperatures were measured. The measured current-voltage data were analyzed by computer fitting using a junction model to obtain parameters. From the computer fitting results, it was confirmed that the recombination process is dominant in the current transport mechanism of the homojunctions in monocrystalline  $\text{CuInSe}_2$ . The relationships between capacitance and voltage, capacitance and frequency were also investigated in detail. It was found that at a given voltage, the capacitance value decreased when the measuring frequency was increased. This result indicated that deep defects exist in the material. Deep level transient spectroscopy (DLTS) measurements were performed on all of the samples in order to investigate the deep levels. Two hole trap levels, one located at  $250 \pm 15$  meV and the other at  $520 \pm 15$  meV from the valence band edge, were observed in the samples treated at  $200^\circ\text{C}$  in  $\text{N}_2$ . For the sample heated at  $200^\circ\text{C}$  in air, the latter was at 850 meV. The above results suggested that O atoms may have an important contribu-

tion to the defects. The electron traps, with the energy at  $182 \pm 14$  meV from the conduction band edge, were found on all of the samples treated in  $N_2$  and air. The average density was about  $6.4 \times 10^{14} \text{ cm}^{-3}$  for the electron traps, and was in the order of  $10^{13} \text{ cm}^{-3}$  for the hole traps.

## Résumé

On a fabriqué des homojonctions en diffusant de l'indium ou du bismuth dans des substrats monocristallins de  $\text{CuInSe}_2$  fabriqué au préalable par la méthode de croissance cristalline verticale de Bridgman. Les caractéristiques courant-tension ont été mesurées à différentes températures. On a alors approximé ces données par des courbes ajustables en utilisant un modèle mathématique de la jonction de manière à obtenir les paramètres caractérisant la jonction. A partir de ces paramètres on a pu confirmer que la recombinaison de porteurs de charge est le mécanisme dominant du transport du courant dans les homojonctions de  $\text{CuInSe}_2$  monocristallin. On a aussi étudié en détail les relations entre la capacité et la tension, et entre la capacité et la fréquence. On a trouvé qu'à une tension donnée, la capacité diminuait lorsque la fréquence du signal alternatif était augmentée. Ceci indique l'existence de niveaux profonds dans le matériau. On a donc effectué des mesures de spectroscopie des niveaux profonds par mesures de capacités transitoires (DLTS) sur tous les échantillons de manière à caractériser les niveaux profonds ainsi mis en évidence. Dans les échantillons traités à  $200^\circ\text{C}$  dans une atmosphère d'azote, on a observé deux niveaux de pièges à trous, dont un situé à  $250 \pm 15$  meV et l'autre à  $520 \pm 15$  meV du bord de la bande de valence. Dans les échantillons traités à  $200^\circ\text{C}$  dans l'air, ce dernier niveau de

pièges était à 850 meV. Ces résultats suggèrent que les atomes d'oxygène pourraient jouer un rôle important dans la formation de ces défauts. On a trouvé dans tous les échantillons, traités dans l'air ou dans l'azote, un niveau de pièges à électrons se trouvant à  $182 \pm 14$  meV du bord de la bande de conduction. La densité moyenne de niveaux profonds étaient d'environ  $6.4 \times 10^{14}$  cm<sup>-3</sup> pour les pièges à électrons, et de l'ordre de  $10^{13}$  cm<sup>-3</sup> pour les pièges à trous.

## Acknowledgements

The author wishes to express her sincere appreciation to Dr. I. Shih for his invaluable guidance and assistance through the course of this study. His personal and professional support has made the experience enriching and enjoyable, without which, none of this would have been possible.

The author would also like to thank all of the colleagues in the laboratory for their friendship and helpful discussions, especially to Mr. L.S. Yip, who has provided  $\text{CuInSe}_2$  crystals for the experiments and given suggestions during the work, and Mr. L. Isnard for translating the abstract into French.

The gratitude ever extend to the author's parents and her husband, who always give encouragement, love and balance to her.

## Table of Contents

ABSTRACT	i
RESUME	iii
ACKNOWLEDGEMENTS	v
TABLE OF CONTENTS	vi
CHAPTER 1 INTRODUCTION	1
CHAPTER 2 JUNCTION FABRICATION AND CURRENT-VOLTAGE, CAPACITANCE-VOLTAGE MEASUREMENTS	11
2.1 Junction Fabrication	11
2.2 Junction Theory and Experimental Results	14
2.2.1 Current-Voltage Characteristics	14
2.2.2 Capacitance-Voltage Characteristics	20
CHAPTER 3 PRINCIPLE AND SYSTEM FOR DLTS MEASUREMENTS	46
3.1 Principle of DLTS Measurements	46
3.1.1 The Concept of Deep Levels	46
3.1.2 Capture Rate and Emission Rate	47
3.1.3 Deep Level Parameters and Capacitance Transient	50

3.1.4	DLTS Technique	55
3.2	DLTS System	61
3.2.1	Capacitance Meter	61
3.2.2	Pulse Excitation Unit	62
3.2.3	Signal Processor	62
3.2.4	Cryostat and Temperature Controller	63
3.2.5	Data Recording Unit	64
CHAPTER 4	DLTS MEASUREMENTS ON CuInSe <sub>2</sub> JUNCTIONS	73
4.1	Capacitance Transient for Hole Traps	73
4.2	Hole Trap Parameters	76
4.3	Capacitance Transient for Electron Traps	79
4.4	Electron Trap Parameters	81
CHAPTER 5	CONCLUSIONS	99
REFERENCES		103

## Chapter 1 Introduction

Among various compound materials, the semiconductor copper indium diselenide ( $\text{CuInSe}_2$ ) appears to have a strong potential for practical device applications because of its high optical absorption coefficients and thermal stability. This compound can be used in components involving non-linear optics, light emitting diodes, photovaltaic optical detectors and solar cells. A considerable amount of investigation has been carried out to gain a clear understanding of the crystal structure, the electrical properties as well as the optical properties of this material [1.1]. For the crystalline  $\text{CuInSe}_2$ , it has been shown that there exist two solid state phase transformations [1.2], one at the temperature of  $810^\circ\text{C}$  and the other at  $665^\circ\text{C}$ . The high-temperature phase ( $>810^\circ$ ) is a sphalerite structure and it is a chalcopyrite structure when the temperature is reduced below  $665^\circ\text{C}$ . The lattice constants for the chalcopyrite structure are  $a=5.785\text{\AA}$  and  $c/a=2.00$  at room temperature. The phases existing between  $810^\circ\text{C}$  and  $665^\circ\text{C}$  are presently not well characterized. The melting point of the compound is about  $986^\circ\text{C}$ , and the energy gap is near to 1 eV. Various papers were also published on the electrical and optical characterization of

CuInSe<sub>2</sub>. The electron and hole concentrations, the carrier mobility and the impurity states were investigated in detail by several workers for more than twenty years. Up to now, however, there are still some unanswered questions left for the practical CuInSe<sub>2</sub> devices. For example, the properties of solar cells fabricated using this material were not as good as that expected. Therefore, further studies are necessary for this compound, especially on defects of the material.

It is convenient to study the properties of the compound semiconductor CuInSe<sub>2</sub> by using devices fabricated in substrates in a monocrystalline form rather than in any other forms. In our laboratory, extensive efforts have been made to obtain good quality single crystals [1.6][1.7]. The typical methods to grow the CuInSe<sub>2</sub> crystals are the Bridgman (or Stockbarger) method and liquid encapsulated Czochralski pulling [1.3]-[1.7]. For the Bridgman method [1.6], the materials are sealed in an ampoule which is located in a region with a fixed temperature gradient. After being heated to a temperature above the melting point, the ampoule is moved out of the furnace at a very slow rate to allow for a directional solidification to form a crystal. During the growth using the Stockbarger method, however, the ampoule is kept at a fixed location while the furnace temperature decreases at a selective slow rate. Different from the Bridgman or Stockbarger method, the encapsulated Czochralski pulling [1.4] uses an open crucible. In order to minimize

vaporization of selenium (because of a high vapor pressure), a  $B_2O_3$  liquid encapsulant is applied on top of the melt in conjunction with argon gas. The starting materials used in all of the growth methods can be polycrystals or high-purity elements in a weighed stoichiometric ratio for  $CuInSe_2$ . The ampoule cleaning, material mixing above the melting point and slow cooling of the melt to the temperature below the transition temperature are all critical for obtaining void-free and crack-free single crystal ingots.

The samples used in present work were prepared by the vertical Bridgman method [1.7]. A conventional rf-heated Czochralski crystal pulling system was modified and used for the growth of  $CuInSe_2$ . Before the growth, an accelerated crucible rotation technique was adopted to mix the melt. Using this method, void-free and crack-free ingots of good quality were prepared in our laboratory.

A p-n junction is one of the simplest devices for studying the properties of semiconductor materials. It can be conveniently used for deep level studies by a deep level transient spectroscopy method because the interface state densities in the p-n junction is usually small. In the present work,  $n^+$ -p homojunctions were formed by diffusing indium or bismuth into p-type  $CuInSe_2$  monocrystalline substrates. Unlike  $CdS/CuInSe_2$  heterojunctions, the homojunctions do not have the unwanted interdiffusion of elements such as Cd, S and O. In practical p-n homojunctions, the current vs voltage relation deviates

from the ideal one because of surface effects, deep traps in the material and series resistance. Accordingly, a fitting process was used in the present work to determine the ideality factor ( $n$ ), the series resistance and parallel resistance of the junctions by the aid of a computer. The ideality factor should be equal to 1 for an ideal  $n^+p$  junction. However, for practical  $\text{CuInSe}_2$  junctions, the ideality factors are always greater than 1. This fact implies that deep level defects are present in the monocrystalline  $\text{CuInSe}_2$  grown by the Bridgman method. The deep levels can result in generation and recombination of charge carriers, leading to a greater than 1 ideality factor.

According to the position of defect centers, they can be classified into two categories: shallow and deep energy levels. The shallow levels are close to the band edges with binding energies of the ground state usually less than about 50 meV. Such centers are responsible for free carriers and the electrical conductivity in the semiconductors. The deep levels, however, have binding energies much larger than that of the shallow levels. One of the most important properties of the deep levels is the ability to control minority carrier lifetime in the semiconductors. The minority carrier lifetime plays a critical role in many semiconductor electronic devices. In light emitting devices, semiconductor lasers and switching circuits, it is favorable to reduce the minority carrier lifetime by intro-

ducing the deep levels. In solar cells, however, the efficiency will be reduced substantially if a large number of deep levels is present since the rate of recombination of minority carriers will increase in the depletion region. Therefore, it is very important to investigate the deep levels in solar cell materials such as  $\text{CuInSe}_2$ .

Several techniques have been developed to investigate the defect states in semiconductors [1.8]-[1.21]. The methods can be divided into two main categories: bulk measurement techniques and space charge techniques. The bulk measurement techniques include photo luminescence, optical absorption, Hall effect, photoconductivity and lifetime measurements. One of the advantages of the bulk methods is that the investigation can be made in semiconductor regions where the electric field is small. However, these measurements are always sensitive to shallow defect centers, thus reducing the sensitivity of deep level measurements. Contrarily, the space charge techniques are often much more sensitive for the detection of deep centers. In the space charge methods, the measurements are usually carried out to investigate specifically the depletion region of a Schottky junction or a p-n junction. Typical space charge techniques include thermally stimulated current method (TSC) [1.8][1.9], thermally stimulated capacitance method (TSCAP) [1.13], edge region TSCAP [1.14], admittance spectroscopy [1.10], photocapacitance method [1.17][1.19] and deep level transient spectroscopy (DLTS) [1.20]. The principle of the

thermally stimulated current (TSC) measurement is as follows. The traps are first filled and the semiconductor cooled to a low temperature. After this, the material is heated at a constant rate and the resulting thermally stimulated currents while the traps are being emptied are observed. This method can be used for both bulk and junction measurements. However, the noise in the measurements is often large. The thermally stimulated capacitance method (TSCAP) has better immunity to noise and surface leakage current and has an ability to distinguish between majority and minority carrier traps. With initially filled or emptied traps in the junction depletion region, a relation between the high-frequency small-signal capacitance of the semiconductor junction and the temperature is obtained. The result is used to determine the trap concentration and the thermal activation energies of the trapped electrons and holes. One of the disadvantages of the TSCAP method is that it can not be used effectively for traps with binding energies less than approximately 0.25 eV because the effective rate window of TSCAP is typically on the order of  $0.1 \text{ sec}^{-1}$ . Edge region TSCAP can observe the shallow and intermediate majority carrier traps, but it is much less sensitive than the ordinary TSCAP and thus is limited to semiconductors with a large defect concentration. The photocapacitance method can be used to obtain the required information on deep levels. When light is incident on a junction, carriers are excited in and near the

depletion layer. If the bias voltage is fixed, the differential capacitance of the junction will be affected by the number of traps filled or emptied due to the illumination. This method is relatively sensitive but is not practical since the analysis is too complex. It may be useful for studying optical properties of deep levels. The admittance spectroscopy method is a method which is considered to be spectroscopic. This method can be used to deduce depth of deep levels, capture rate, concentration and type (donor or acceptor) by observing the peaks in ac conductance measured as a function of temperature and frequency. The disadvantage of this method is that it is limited to only majority carrier traps and the sensitivity is low for deeper traps.

The deep level transient spectroscopy (DLTS) is a very accurate and easy method as compared to the methods described above. It is based on the principle of the TSCAP method, with further improvements. It can be used to observe a variety of traps in semiconductors by using a high-frequency (1 MHz) temperature-dependent capacitance transient measurement. The presence of traps is revealed by the presence of a positive or negative peak of DLTS spectrum which is a plot of the difference of capacitance between time  $t_1$  and  $t_2$  versus the temperature. Trap concentration, activation energy and type of traps, as well as capture cross section, can all be obtained from the analysis of the DLTS spectra. The sign of peaks is used to distinguish between majority traps and minority traps. In the

thesis, the DLTS method is used for studying properties of traps in monocrystalline  $\text{CuInSe}_2$ .

Research experiments on deep levels in  $\text{CuInSe}_2$  have been reported by several researchers. These experiments can be classified into two categories, one is on thin film solar cells fabricated on polycrystalline  $\text{CuInSe}_2$  and the other is on cells fabricated using bulk monocrystalline  $\text{CuInSe}_2$  samples. For thin film solar cells, Eron and Rothwarf [1.22] have reported a deep hole trap level located at 800 meV from the valence band edge by carrying out temperature dependent single shot capacitance transient measurements on a  $\text{CdZnS/CuInSe}_2$  cell. Fabick and Eskenas [1.23] found a single hole trap level at 237 meV from the valence band edge using an admittance spectroscopy method on  $\text{ZnO/CdS/CuInSe}_2$  cells. Using the deep level transient spectroscopy method, two electron trap levels, one at 78 meV and the other at 135 meV below the conduction band edge, were observed by Ahrenkiel [1.24][1.25] on a  $\text{CdZnS/CuInSe}_2$  thin film cell without an air treatment. The DLTS method is also used by Christoforou and Leslie [1.26] on thin film  $\text{CdS/CuInSe}_2$  cells. They reported a single hole trap level at 700 meV above the valence band edge and an electron trap level at 350 meV from the conduction band edge. The density of their hole traps was  $5 \times 10^{14} \text{ cm}^{-3}$  and was  $3 \times 10^{13}$  for electron traps. For homojunctions cells fabricated using monocrystalline  $\text{CuInSe}_2$ , Qiu and Shih [1.27] detected a very slow decay with a

time constant of about 2 seconds by the single shot transient capacitance method. Hanak and coworkers [1.25] have performed DLTS measurements on a CdZnS/CuInSe<sub>2</sub> cell fabricated on a Bridgman-grown monocrystalline CuInSe<sub>2</sub> substrate. A hole trap level located at 475 meV from the valence band edge was observed using a standard DLTS analysis. This level was reported to consist of two components using a two-trap analysis method: one was at 423 meV and the other at 498 meV from the valence band edge. Using the electrical resistance and Hall effect measurements on n-type monocrystalline CuInSe<sub>2</sub> samples, Neumann [1.28] have detected a deep donor level at 220 meV below the conduction band edge. Using the same method, Iric, Endo and Kimura [1.29] found a donor level at 180 meV from the conduction band edge on bulk n-type CuInSe<sub>2</sub> crystals. Recently, Sobotta and coworkers [1.30] found a deep donor level located at 225 meV from the conduction band edge in as-grown bulk n-type CuInSe<sub>2</sub> samples and a deep acceptor state at 400 meV from valence band edge by photoconductivity measurements.

The experiments carried out in the present work are on homojunctions fabricated by Bridgman grown monocrystalline CuInSe<sub>2</sub>. Before the DLTS measurements, current-voltage and capacitance-voltage measurements were carried out on n<sup>+</sup>p junctions made by diffusing indium or bismuth. DLTS measurements were then made to investigate the parameters of hole traps and electron traps in the monocrystalline CuInSe<sub>2</sub>.

In chapter 2 of the thesis, results of current versus

voltage measurements and differential capacitance versus voltage measurements are first presented. The principle and the system of DLTS method are then given in chapter 3. In chapter 4, both transient decay and DLTS measurements are described. Conclusions of the present research work are finally given in chapter 5.

## Chapter 2 Junction Fabrication and Current-Voltage, Capacitance-Voltage Measurements

### 2.1 Junction Fabrication

Samples of monocrystalline  $\text{CuInSe}_2$ , which were cut from ingots grown by the vertical Bridgman method [1.7], were used to fabricate the homojunctions for the experiments. The growing procedure of the ingots was as follows. First of all, a quartz tube (diameter 1.2 cm) with a sealed end of conical shape was prepared, cleaned and flame-polished for use as an ampoule. High purity starting materials of Cu (99.999%), In (99.999%) and Se (99.999%) were weighed to a ratio for growing  $\text{CuInSe}_2$  (Cu:In:Se=0.92:1.08:2.08) and introduced into the quartz tube. The quartz tube which contained the starting materials was then sealed under a pressure of about  $5 \times 10^{-4}$  Torr to form the ampoule. A quartz rod with a diameter of 0.5 cm was joined to the sealed end of the ampoule and used as a driving rod. The ampoule was inserted into the chamber of an rf-heated furnace so that the starting materials were located in the zone with the highest temperature. In order to avoid the breakage of the ampoule and even an explosion, the materials were first heated

quickly to 200°C and maintained at this temperature for 4 hours. Then the temperature was increased slowly to 450°C at a rate of 20°C/h. Following this, the heating rate was increased to 60-80°C/h until the temperature in the central zone reached 1100°C. At this temperature, all of the starting materials were completely melted. The ampoule with the materials was kept at this temperature for 2 hours, and in the meanwhile, it was rotated using the accelerated crucible rotation technique (ACRT). Both acceleration and deceleration periods were 4 s and with a maximum rate of 5 rpm/s. After a mixing period of 2 hours, the ampoule was withdrawn at a speed of 1-2 mm/h for about 50 hours. When the temperature of the CuInSe<sub>2</sub> melt reached the melting point of this material, solidification began. Then the temperature of the furnace was decreased at the rate of 4-30°C/h. Once the temperature of the materials was below the low phase transition temperature (665°C), the rate of decrease was increased to 60-80°C/h until the CuInSe<sub>2</sub> reached room temperature. Using the above described process, p-type void-free and crack-free crystal grains with an area of about 50 mm<sup>2</sup> and a thickness of more than 5 mm could be selected from the ingots. In the main part of the ingots, the elemental ratio was near to Cu:In:Se=1:1:2. Room temperature Hall-effect measurements showed that the largest mobility value was 73 cm<sup>2</sup>V<sup>-1</sup>s<sup>-1</sup> and the typical value was about 50 cm<sup>2</sup>V<sup>-1</sup>s<sup>-1</sup>. The acceptor concentration was near to 10<sup>15</sup> cm<sup>-3</sup>.

Homojunctions were then fabricated on the p-type monocrys-

talline  $\text{CuInSe}_2$  substrates with a thickness of 1 mm. First, the samples were polished by  $\text{Al}_2\text{O}_3$  powder and rinsed in ACE (acetone) and TCE (trichloroethylene) for 2 minutes. After the rinsing, the samples were etched in a saturated solution of  $\text{K}_2\text{Cr}_2\text{O}_3$  in  $\text{H}_2\text{SO}_4$  (1:9 by weight) at room temperature for 5 minutes. Following the etching process, the samples were thoroughly washed in deionized water and dried. After the drying, the samples were loaded immediately into the chamber of a vacuum system for indium or bismuth evaporation. The chamber was evacuated to a pressure of  $10^{-5}$  Torr by a rotary pump and a diffusing pump before the evaporation. High purity indium or bismuth (59's and 69's respectively) was chosen and evaporated on the substrates through a metal mask having circular windows with an area of  $0.5 \text{ mm}^2$ . The thickness of the evaporated In or Bi layer was about  $2 \mu\text{m}$ . After the evaporation, one of the samples was selected to put into the quartz chamber of a horizontal furnace set at  $200^\circ\text{C}$  for In or Bi diffusion. In order to avoid contamination from the environment, a flow of  $\text{N}_2$  was maintained during the diffusion process. As a result of the diffusion process, the surface layer of  $\text{CuInSe}_2$  was converted from p-type to  $\text{n}^+$ -type and an  $\text{n}^+\text{p}$  homojunction was formed near the surface. The junction depth was controlled by the diffusion time and a value of about  $10 \mu\text{m}$  was obtained after the 20 minute diffusion. In the initial stage of the present work, about 15 samples were fabricated and tested to establish the

appropriate fabrication conditions. In the second stage, the samples described below were specifically fabricated using the procedure obtained and the results are presented in this thesis. Three samples, LH51, LH52 and LH53, involving In diffusion, were treated for 10 minutes, 20 minutes and 40 minutes respectively. Two other samples, LH55 and LH56, were made by diffusing Bi with diffusion times of 10 minutes and 20 minutes, respectively. Another sample again involving In diffusion, LH54, was treated at 200°C for 20 minutes in air for comparison. Table 2.1 gives the fabrication conditions for all of the n<sup>+</sup>p homojunctions used in the present studies. After the diffusion, the back surface of the substrate was polished using a fine sand paper. A layer of Ag paste was applied to the polished back surface and the sample was treated at 50°C in vacuum for about 5 minutes to form a back ohmic contact. Ohmic contacts in the n<sup>+</sup>-side were made directly on the indium or bismuth surface or by soldering conducting wires using Wood's metal.

## **2.2 Junction Theory and Experimental Results**

### **2.2.1 Current-Voltage Characteristics**

The ideal current-voltage characteristics of a semiconductor junction are obtained on the basis of the following four assumptions: (1) abrupt depletion layer approximation, (2) Boltz-

mann approximation, (3) low injection assumption and (4) no generation and recombination current exists in the depletion layer. Shockley [2.1] established the formula describing the J-V relationship for an ideal p-n junction.

$$j = j_0(e^{\frac{qV}{KT}} - 1) \quad 2.1$$

where  $j_0$  is the reverse saturation current density and is given by

$$j_0 = \frac{qD_p p_{p0}}{L_p} + \frac{qD_n n_{n0}}{L_n} \propto T^{(3+\frac{\tau}{2})} \cdot e^{-\frac{E_g}{KT}} \quad 2.2$$

Here,  $D_p$  and  $L_p$  are the hole diffusion coefficient and diffusion length,  $D_n$  and  $L_n$  are the electron diffusion coefficient and diffusion length,  $\tau$  is a constant and  $E_g$  is the energy gap. Fig. 2.1 shows the ideal I-V characteristics of a junction in a semilog plot.

In a practical junction, defects (or traps) are often found to exist in the depletion region. With the presence of the defects, recombination of free carriers may occur in the depletion region under forward bias because of a carrier capturing process. Under reverse bias, generation of carriers occurs in the depletion region where the carrier concentration

is small. The generation current and recombination current are proportional to the intrinsic carrier density,  $n_i$ , which varies with temperature in a form of  $T^{3/2}\exp(-E_g/2KT)$  [2.2]. Therefore, the transport mechanism of the total current is a mixture of diffusion and recombination-generation. The reverse saturation current should be the summation of  $j_0$  (ideal value) and the generation current. In addition, effects of the surface and traps in the depletion layer will result in a leakage current. The action of the total reverse current can be characterized as a shunt resistance. In forward bias, the total current is the summation of the recombination current and the diffusion current. The J-V characteristics of the junction with the recombination current can be given by an expression similar to Eqn. 2.1 with an ideality factor  $n$  larger than unity. Apart from the correction of the shunt resistance and ideality factor, contact resistance and substrate resistance, as well as the resistance from measurement circuits, give rise to an equivalent series resistance. As a result, the real I-V relation in a p-n junction under a dark condition can be depicted as:

$$I = I_0 \exp\left(\frac{q(V-IR_s)}{nKT} - 1\right) + \frac{V-IR_s}{R_{sh}} \quad 2.3$$

Where  $I_0$  is the reverse saturation current,  $R_s$  is the series resistance,  $R_{sh}$  is the shunt resistance and  $n$  is the ideality factor. An equivalent circuit of a practical p-n

junction is shown in Fig. 2.2. The ideality factor  $n$  is equal to 1 when the diffusion current is dominant and equal to 2 when the recombination current is dominant. If both currents are comparable,  $n$  has a value between 1 and 2.

The dark I-V characteristics of the homojunctions have been measured at room temperature using a Hewlett-Packard model 4145A semiconductor parameter analyzer. Fig. 2.3 gives a dark I-V curve of the sample LH54. The breakdown voltage of the sample is larger than 5 V and the leakage current is about several  $\mu\text{A}$ . The current-voltage characteristics at different temperatures were also obtained on the devices. The sample to be tested was loaded in the cooling stage of a cryostat, the temperature of which was regulated by a temperature controller. The sample temperature was controlled to  $\pm 1$  K in the range from 175 K to 300 K by the controller with flowing cold nitrogen. The forward dark I-V characteristics of all homojunctions at different temperatures were measured by the Hewlett-Packard model 4145A semiconductor parameter analyzer and recorded by an IBM personal computer. Fig. 2.4 and Fig. 2.5 show experimental results for the samples LH53 and LH55. It can be seen that the experimental curves deviate from the ideal ones because of the presence of series resistance, shunt resistance and deep traps, yielding an ideality factor  $n$  value which is greater than 1. The series resistance  $R_s$  has a significant effect under large forward bias conditions. But, at a small forward bias,

the shunt resistance dominates the deviation. Usually, the series resistance  $R_S$  and the shunt resistance  $R_{Sh}$  are determined by measuring the differential conductance at high forward and reverse bias, respectively. This method is not very accurate because of a voltage-dependent nature of  $R_S$  and  $R_{Sh}$ . The procedure adopted in the present work is a computer curve fitting which is used to determine the values for  $R_S$  and  $R_{Sh}$ . The fitting method is the least square fitting using Eqn. 2.3. The estimate for the  $\tilde{I}_i$ , which is calculated using Eqn. 2.3 with the measured data, is compared with the experimental value  $I_i$ . The fitting values of  $R_S$ ,  $R_{Sh}$ ,  $n$  and  $I_0$  are determined by minimizing the sum of the squares of the current residuals,  $m$ .

$$m = \sum_{i=1}^N (I_i - \tilde{I}_i)^2 \quad 2.4$$

Where  $N$  is the total number of data pairs. Fig. 2.6 and Fig. 2.7 illustrate the fitting results for the sample LH53 and LH55 in the temperature range from 175 K to 300 K. The experimental current-voltage curves are also shown in Fig. 2.6 and Fig. 2.7 for comparison. It is clear that the curves from the fitting are quite close to the experimental ones. Table 2.2 and Table 2.3 give the detail calculated values of  $R_S$ ,  $R_{Sh}$ , ideality factor  $n$  and reverse saturation current  $I_0$  at different temperatures.

From the fitting results, it is evident that the reverse

saturation current  $I_0$  is dependent on the temperature. As the temperature is decreased,  $I_0$  decreases. This is obvious if the Eqn. 2.2 is considered where the temperature dependence of the term  $T^{(3+\tau/2)}$  is not important when compared with the exponential term. Therefore, the reverse saturation current is proportional to  $\exp(-E_g/KT)$ . Moreover, the generation current decreases when the temperature is decreased. From the fitting values, it was also found that the series resistance ( $R_s$ ) is dependent on the temperature. The lower the temperature is, the higher the value of  $R_s$  becomes. This implies that the device contact resistance and the resistance in the measurement circuit are not dominant in the series resistance and it is the semiconductor bulk resistance which give the main contribution to the series resistance. Besides, non-ohmic contacts may occur at low temperatures.

According to the fitting results, the shunt resistance increases when the temperature is decreased. This effect is due to the reduction of the leakage current at low temperatures since the traps become less active. The ideality factors  $n$  at different temperatures obtained from the fitting results are near to 2 for the sample LH53. The  $n$  factor show a slight increase when the temperature is reduced. The reason for the slight increase in  $n$  is that the recombination process are more important at low temperatures. For the sample LH55 which was formed by a 10 minute Bi diffusion, the fitting results show

that the values of the ideality factor are larger than 2. This may be due to a tunneling effect which is not included in the equation 2.3. Apart from the recombination, defects in the depletion layer will result in the tunneling effect if the depletion region is narrow. If the tunneling effect is included, the equation for the I-V characteristics of a junction should be corrected as:

$$I = I_0(\exp C(V-IR_s)-1) + \frac{V-IR_s}{R_{sh}} \quad 2.5$$

Where  $C=(1-f)B+f/nKT$ , B is a tunneling parameter and f is the degree of tunneling character [2.3][2.4][2.5].

## 2.2.2 Capacitance-Voltage Characteristics

Capacitance-voltage (C-V) measurement technique is an essential method for studying junction properties such as the doping concentration, the defect density and the barrier height. When a p-type semiconductor material is joined to an n-type material to form a p-n junction, electrons diffuse from the n-type material to the p-type one and holes move from the p-type material to the n-type material because of the difference of carrier concentration between the n and p regions. The diffusion of charge carriers results in a space charge region with

an associated electric field which forces the electrons to drift back to the n-type region and the holes back to the p-type region. If the diffusion action is canceled by the drift action, a thermal equilibrium is reached and the net flow of carriers is zero. The charged region near the metallurgical junction where the mobile carriers have been reduced is called the depletion region. Normally, when the deep traps are ignored, the total charge in the depletion region can be expressed as:

$$\rho(x) = q \cdot (p(x) - n(x) + N_D^+(x) - N_A^-(x)) \quad 2.6$$

where  $p(x)$  and  $n(x)$  are the hole and electron concentrations,  $N_D^+(x)$  and  $N_A^-(x)$  are the ionized impurity concentrations. If we consider a one-sided abrupt p-n junction with  $N_D \gg N_A$  and assume that the impurity atoms are totally ionized, then the equation 2.6 can be simplified to equation 2.7.

$$\rho(x) = -q \cdot (N_A^-(x) - p(x)) \quad 2.7$$

Using the Poisson's equation, the depletion width can be derived as

$$W = \sqrt{\frac{2\epsilon_s(V_{bi} \pm V - 2KT/q)}{qN_B}} \quad 2.8$$

where  $N_B$  is equal to  $N_A$  in the p-type material,  $V_{bi}$  is the built-in potential,  $V$  is the voltage applied across the two terminals of the junction and  $\epsilon_s$  is the permittivity of the semiconductor.

The total charge per unit area in the depletion layer is:

$$Q = qN_B W \quad 2.9$$

For one-sided abrupt junctions, the capacitance per unit area is given by

$$\begin{aligned} C &= \frac{dQ}{dV} \\ &= \frac{d(qN_B W)}{d(qN_B W^2 / 2\epsilon_s)} \\ &= \sqrt{\frac{q\epsilon_s N_B}{2}} \cdot (V_{bi} \pm V - 2KT/q)^{-\frac{1}{2}} \end{aligned} \quad 2.10$$

So,

$$\frac{1}{C_2} = \frac{2}{q\epsilon_s N_B} \cdot (V_{bi} \pm V - 2KT/q) \quad 2.11$$

and

$$\frac{d\left(\frac{1}{C^2}\right)}{dV} = \frac{2}{q\epsilon_s N_B} \quad 2.12$$

It is clear from equation 2.12 that a straight line should be resulted in the  $1/C^2$  versus  $V$  plot for the one-sided abrupt junction. The slope of the plot is inversely proportional to the impurity concentration of the substrate,  $N_B$ . From the voltage intercept of the plot ( $1/C^2=0$ ), information on the band bending of the junction can be obtained.

If deep levels with a density  $N_T$  exist in the material, the depletion charge will be affected due to ionization of the traps. Therefore, the junction capacitance under this condition is affected by the ionization states. Fig. 2.8 shows the electronic structures of a reverse-biased  $p^+-n$  junction with single deep level (donor like or accept like). Where  $V_R$  is the applied reverse bias,  $E_C$  is the position of the conduction band edge,  $E_D$  is the shallow donor level,  $E_F$  is the Fermi level,  $E_T$  is the trap level,  $Y$  is the point at which  $E_F$  and  $E_T$  intersect, and  $W$  is the edge of the depletion region. The capacitance at a given frequency are directly related to the two depleted regions: transition region and space charge region.

Generally, the capacitance of a junction is measured by applying a small AC voltage on a fixed DC voltage across the junction. The frequency of the small AC voltage has a strong effect on the junction capacitance when deep levels are present in the depletion region. At low frequencies, the ionization states of deep centers can follow the AC voltage change. The capacitance is therefore determined by the sum of deep and shallow impurities. However, at high frequencies, because of

the long time constant of deep centers (which is determined by emission rates with a typical value of  $10^{-3}$  sec), only shallow impurities (with a time constant in the range  $10^{-6}$ - $10^{-9}$  sec) can charge and discharge responding to the AC voltage. At intermediate frequencies, some of the deep centers with the time constants short enough are also able to follow the AC voltage and contribute to the capacitance. As a result, the higher the AC frequency is, the smaller the capacitance will be at a fixed bias voltage. The degree of capacitance variation between the high and low frequencies at a given reverse voltage is therefore dependent on the density and energy of the defects.

Dark capacitance-voltage measurements at different frequencies have been carried out on all of the  $\text{CuInSe}_2$  homojunctions used in the present work. The samples were loaded into a dark box and the C-V characteristics measured using a Hewlett-Packard 4274A multi-frequency LCR meter. The reverse bias was monitored by a Hewlett-Packard 3428A multimeter and the measured data was recorded by an IBM personal computer. The measurements were carried out at five frequencies in the range from 4 KHz to 100 KHz. The reverse bias range used in the measurements was from 0 to 3 V with steps of 0.5 V. Fig. 2.9 and Fig. 2.10 show results of the capacitance versus voltage measurements for the samples LH52 and LH56. It can be seen that the variation of capacitance from the low frequencies to the high

frequencies at a fixed reverse bias for the sample LH52 has not apparent difference from that for the sample LH56. This fact suggests that density of deep levels in the sample LH56, which was made by diffusing Bi into p-type  $\text{CuInSe}_2$ , is nearly equal to that in the sample LH52, which was formed by In diffusion. In Fig. 2.9 and Fig. 2.10, it is also seen that the capacitance variation with frequency is smaller at larger reverse bias voltages. This phenomenon is consistent to the analysis using the Sah-Reddi model [2.6].

The  $1/C^2$  versus  $V$  curves can be used to obtain the impurity density in the depletion region. The  $1/C^2$  versus  $\sqrt{V}$  curves are shown in Fig. 2.11 and Fig. 2.12 for the sample LH52 and LH56. It is noted that the curves are not linear and the slopes at small reverse bias voltages are greater than that at large reverse bias voltages. The fact indicates that the impurity density is not uniform in the depletion region in the present devices. Near the interface of the junctions, the impurity concentration is small. This is reasonable considering compensation of acceptors by donors in the surface region. The nonuniform impurity concentration distribution will affect the determination of trap density (to be described in chapter 4). The impurity densities at two different frequencies (10 KHz and 100 KHz) for all of the samples were calculated at a certain depth by the computer and the results are given in Table 2.4. From the results shown in Table 2.4, it is evident that deep levels are present in all of the samples.

The relationship between capacitance and frequency was studied in the range from 500 Hz to 2 MHz. At low frequencies, the capacitance was large since deep centers can respond to the AC voltage. Small capacitance values were observed at relatively high frequencies because only shallow donors and the deep levels with short time constants can follow the AC voltage. The larger the change of the capacitance from a low to a high frequency is, the higher the defect density is. Results of measurements for the samples LH52, LH53 and LH54 are presented in Fig. 2.13. Fig. 2.14 gives results of the measurements for the samples LH55 and LH56. Although the change of magnitude in capacitance with the change of frequency is different for different samples, the tendency is the same. It is also noted that there is no apparent steps in all of the capacitance-frequency curves. This fact suggests that the deep levels in the  $\text{CuInSe}_2$  have different time constants.

Based on the studies of I-V and C-V characteristics on the  $\text{CuInSe}_2$  homojunctions, it is thus concluded that deep levels indeed exist in this material. Detailed information about the deep defects such as energy levels, densities and capture cross sections are difficult to obtain from the I-V and C-V measurements. In order to obtain such information, deep level transient spectroscopy (DLTS) should be used to analyze the material. In the following chapters, the principle and system for the DLTS measurements will be described and the results of

deep level studies on the  $\text{CuInSe}_2$  homojunctions using the DLTS will be presented.

Table 2.1 Fabrication conditions for all CuInSe<sub>2</sub> homojunctions.

Sample No.	Doping Source	Gas in Chamber	Diffusion Time (min.)	Diffusion Temperature (°C)
LH51	In	N <sub>2</sub>	10	200
LH52	In	N <sub>2</sub>	20	200
LH53	In	N <sub>2</sub>	40	200
LH54	In	air	20	200
LH55	Bi	N <sub>2</sub>	10	240
LH56	Bi	N <sub>2</sub>	20	200

Table 2.2 Parameters obtained from fitting of the I-V curves for the sample LH53.

Temperature (k)	$I_0$ (Amp.)	$R_s$ ( $\Omega$ )	$R_{sh}$ ( $\Omega$ )	Ideality (n) Factor
175	$5.83 \times 10^{-12}$	$1.25 \times 10^5$	$5 \times 10^9$	2.26
200	$5.70 \times 10^{-11}$	$2.76 \times 10^4$	$9 \times 10^8$	2.14
225	$4.49 \times 10^{-10}$	$7.01 \times 10^3$	$5 \times 10^8$	1.99
250	$3.62 \times 10^{-9}$	$1.96 \times 10^3$	$8 \times 10^7$	1.94
275	$2.34 \times 10^{-8}$	$6.51 \times 10^2$	$4 \times 10^7$	1.90
300	$1.23 \times 10^{-7}$	$2.99 \times 10^2$	$1 \times 10^7$	1.89

Table 2.3 Parameters obtained from fitting of the I-V curves for the sample LH55.

Temperature (K)	$I_0$ (Amp.)	$R_S$ ( $\Omega$ )	$R_{sh}$ ( $\Omega$ )	Ideality Factor
175	$4.27 \times 10^{-11}$	$4.08 \times 10^4$	$6.29 \times 10^7$	3.26
200	$3.16 \times 10^{-10}$	$1.24 \times 10^4$	$1.12 \times 10^7$	3.00
225	$3.87 \times 10^{-9}$	$3.25 \times 10^3$	$2.95 \times 10^6$	2.98
250	$3.46 \times 10^{-8}$	$9.24 \times 10^2$	$8.41 \times 10^5$	3.01
275	$2.67 \times 10^{-7}$	$3.15 \times 10^2$	$6.65 \times 10^5$	3.12
300	$1.37 \times 10^{-6}$	$1.43 \times 10^2$	$5.60 \times 10^5$	3.17

Table 2.4 Comparison of the densities at two different frequencies.

Sample No.	Concentration ( $\text{cm}^{-3}$ )		Dist. from Junction ( $\mu\text{m}$ )	$N_{10\text{K}} - N_{100\text{K}}$
	10 KHz	100 KHz		
LH51	$1.32 \times 10^{15}$	$7.55 \times 10^{14}$	2.0	$5.6 \times 10^{14}$
LH52	$6.48 \times 10^{14}$	$4.94 \times 10^{14}$	3.0	$1.5 \times 10^{14}$
LH53	$1.77 \times 10^{15}$	$4.61 \times 10^{14}$	3.0	$1.3 \times 10^{15}$
LH54	$7.25 \times 10^{14}$	$4.15 \times 10^{14}$	3.0	$3.1 \times 10^{14}$
LH55	$5.9 \times 10^{14}$ (20K)	$2.00 \times 10^{14}$	2.1	$3.9 \times 10^{14}$
LH56	$6.35 \times 10^{14}$	$5.43 \times 10^{14}$	2.0	$9.2 \times 10^{13}$

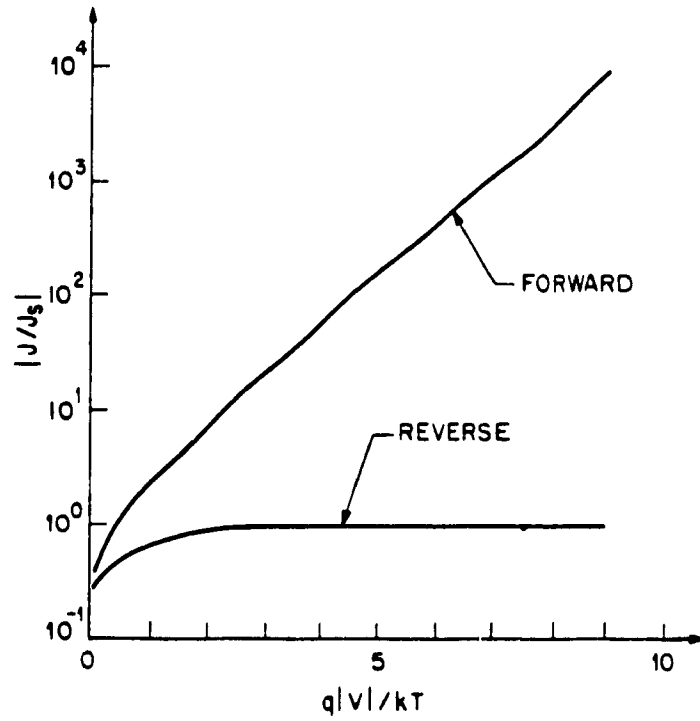


Fig.2.1 Ideal I-V characteristics of a p-n junction.

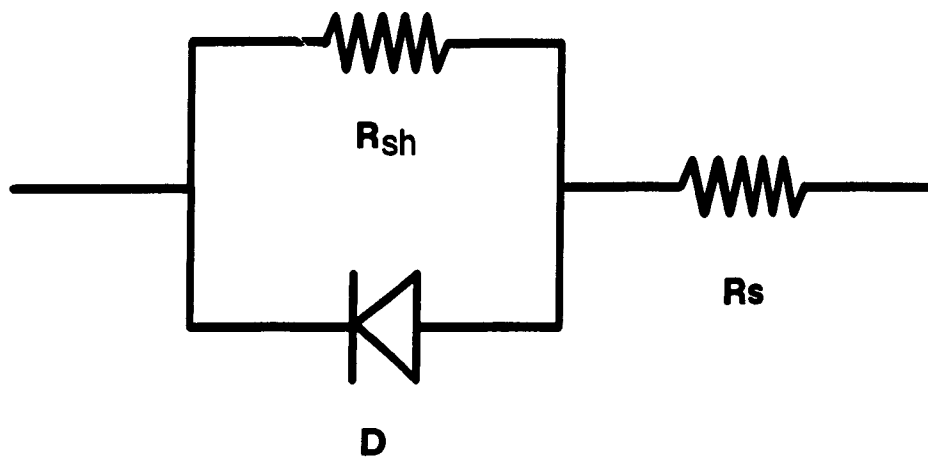


Fig.2.2 An equivalent circuit of the practical p-n junction.

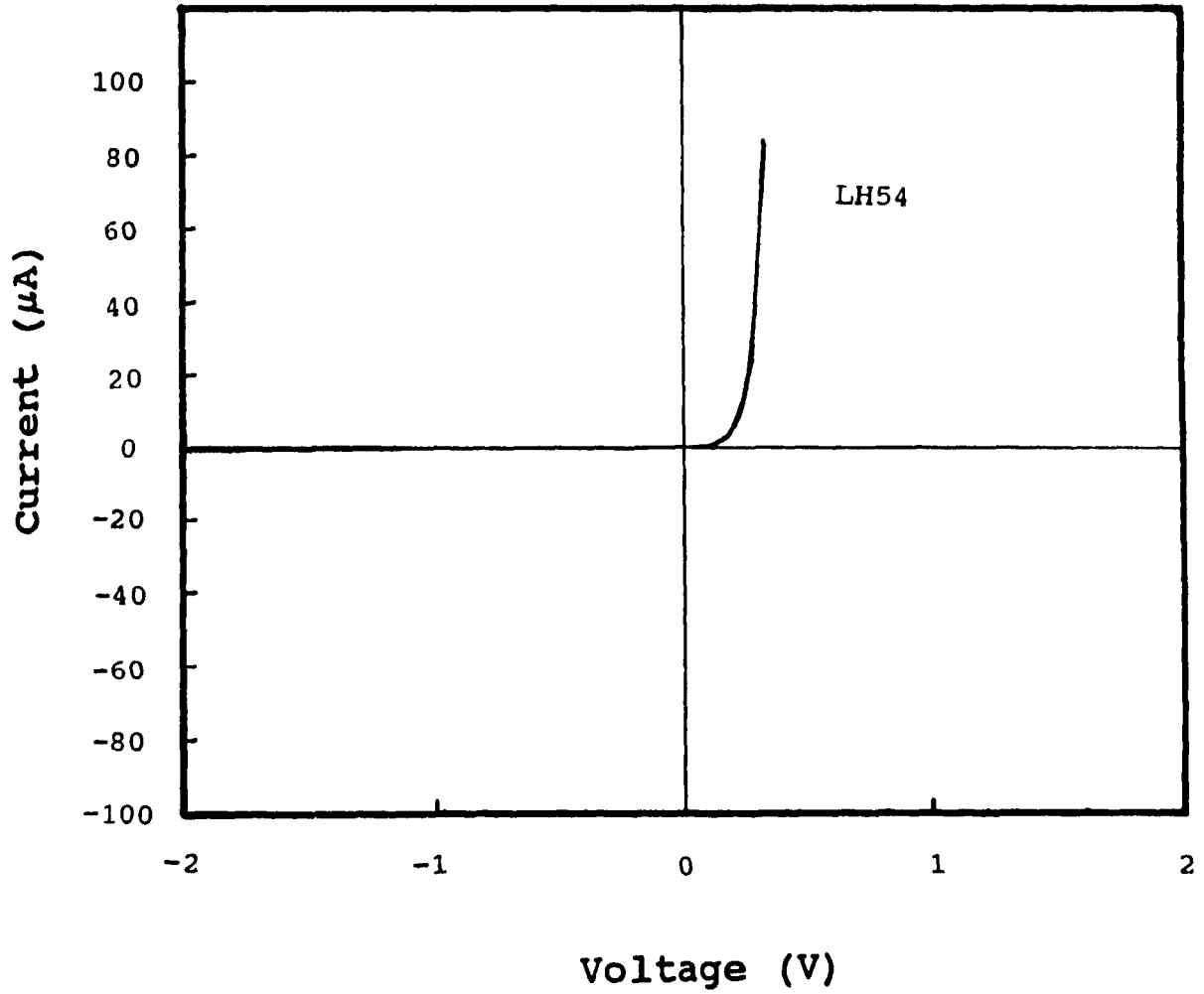


Fig.2.3 Dark I-V characteristics of the sample LH54 at 300 K.

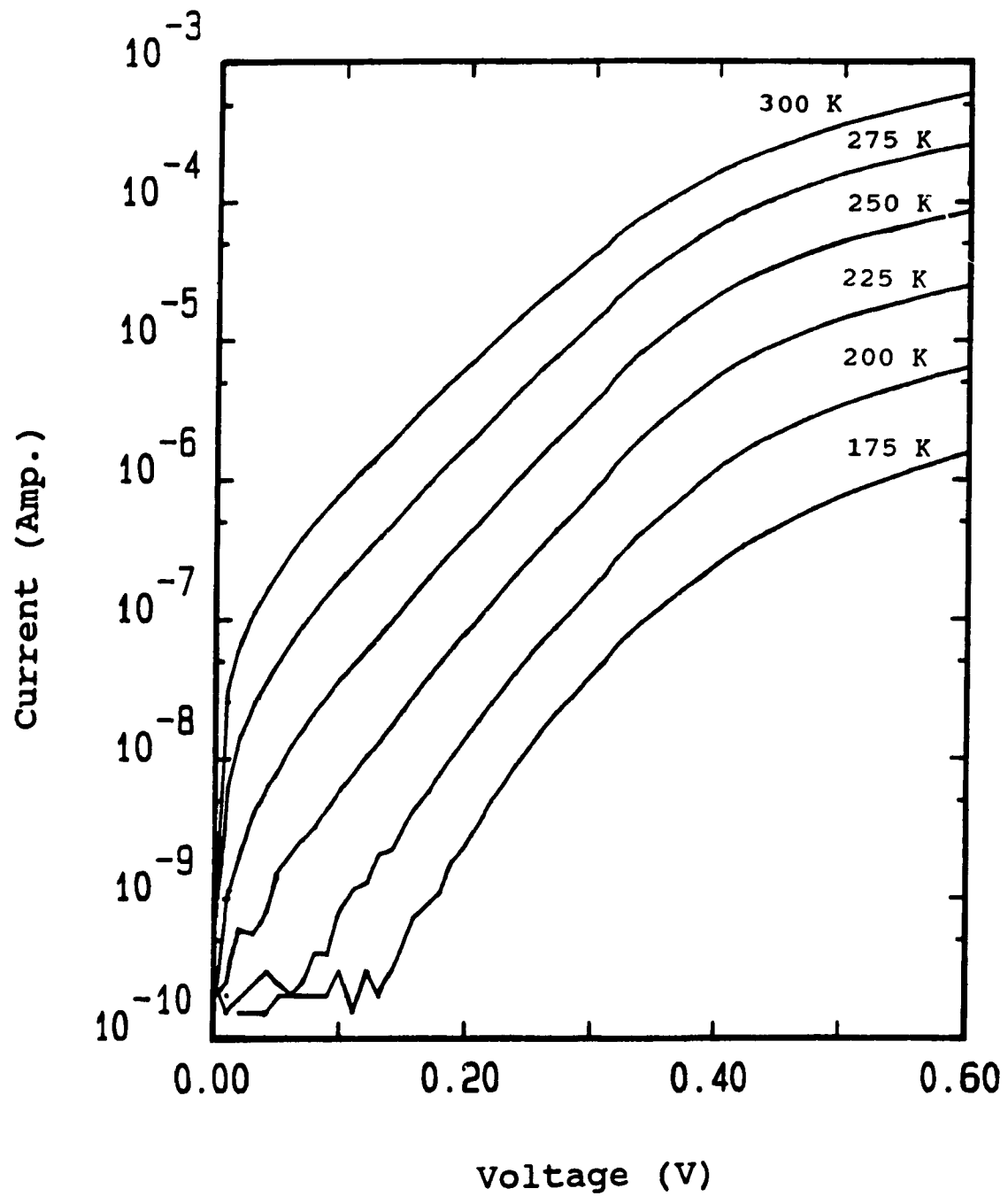


Fig.2.4 Forward dark I-V characteristics of the sample LH53 at different temperatures.

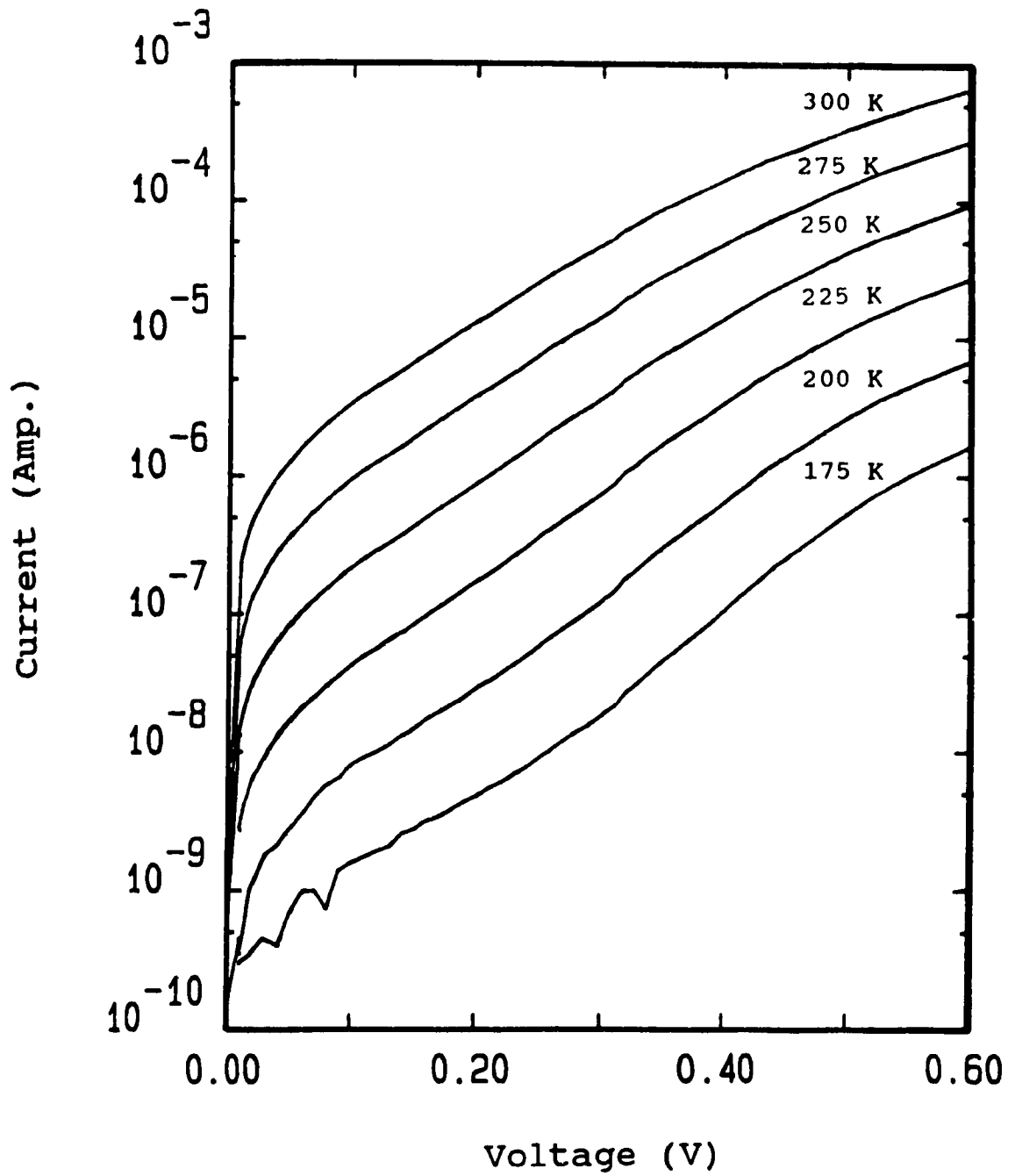


Fig.2.5 Forward dark I-V characteristics of the sample LH55 at different temperatures.

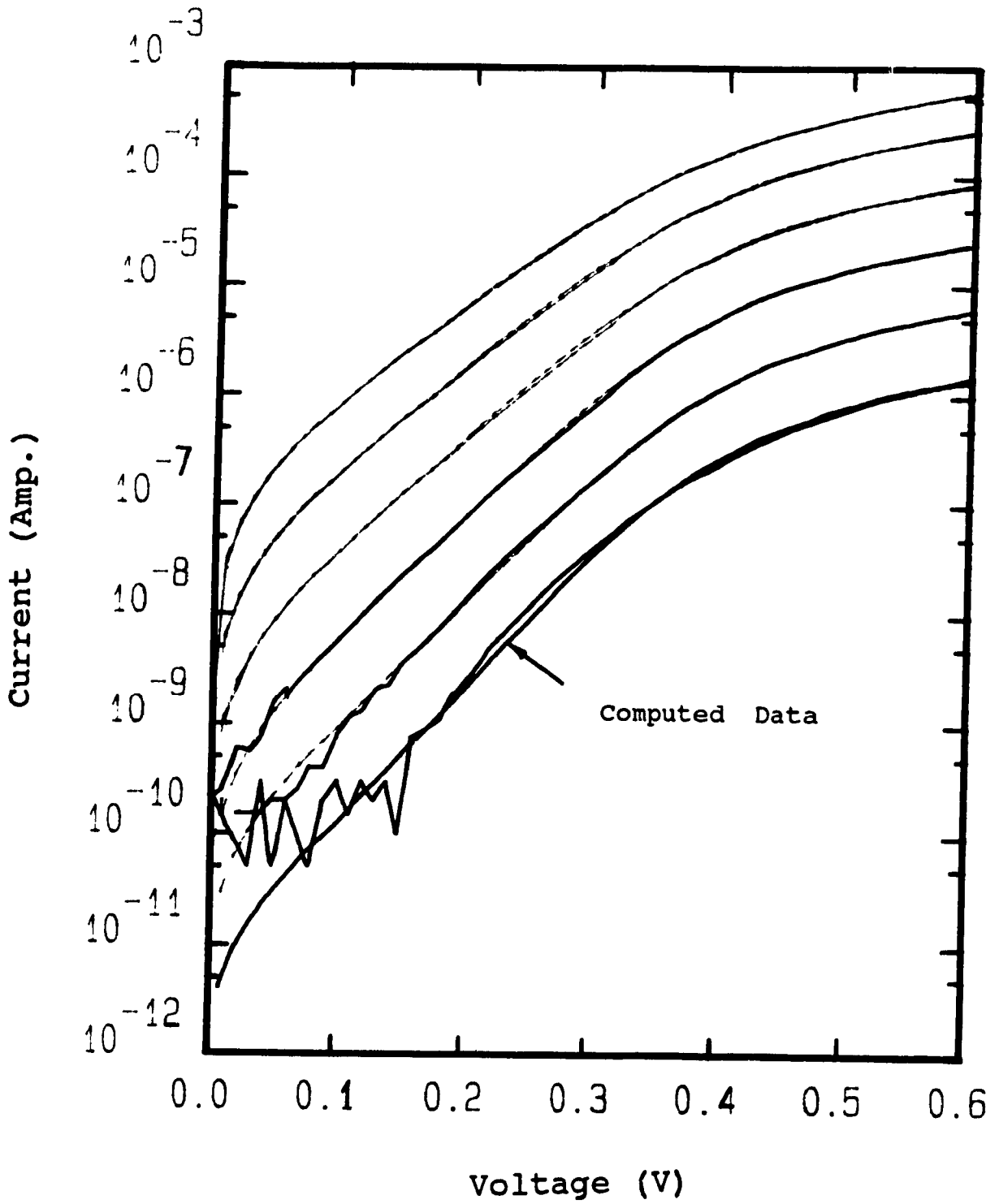


Fig.2.6 Plots of the measured I-V curves and the computed data for the sample LH53.

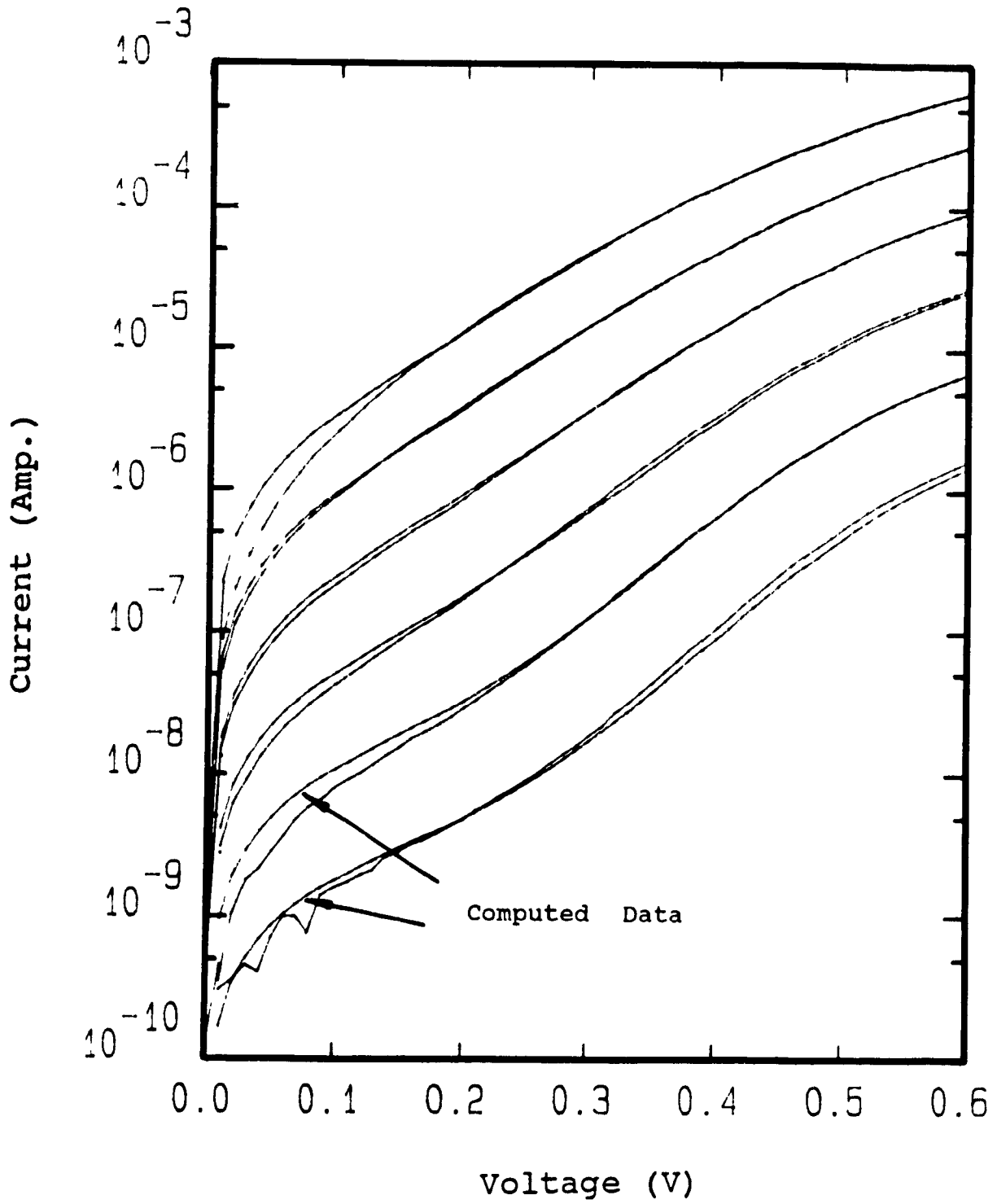


Fig.2.7 Plots of the measured I-V curves and the computed data for the sample LH55.

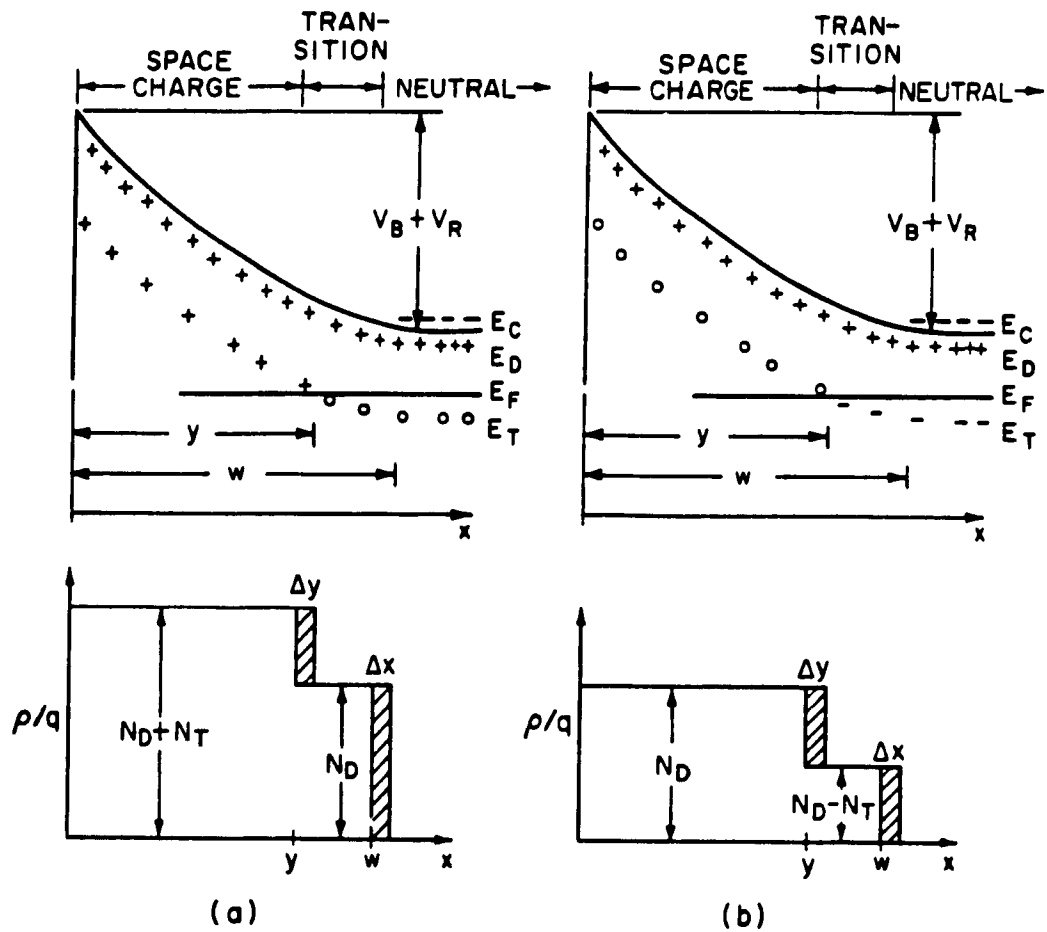


Fig.2.8 Electronic structures of a reverse-biased  $p^+-n$  junction with single deep level: (a) Deep donor traps; (b) Deep acceptor traps.

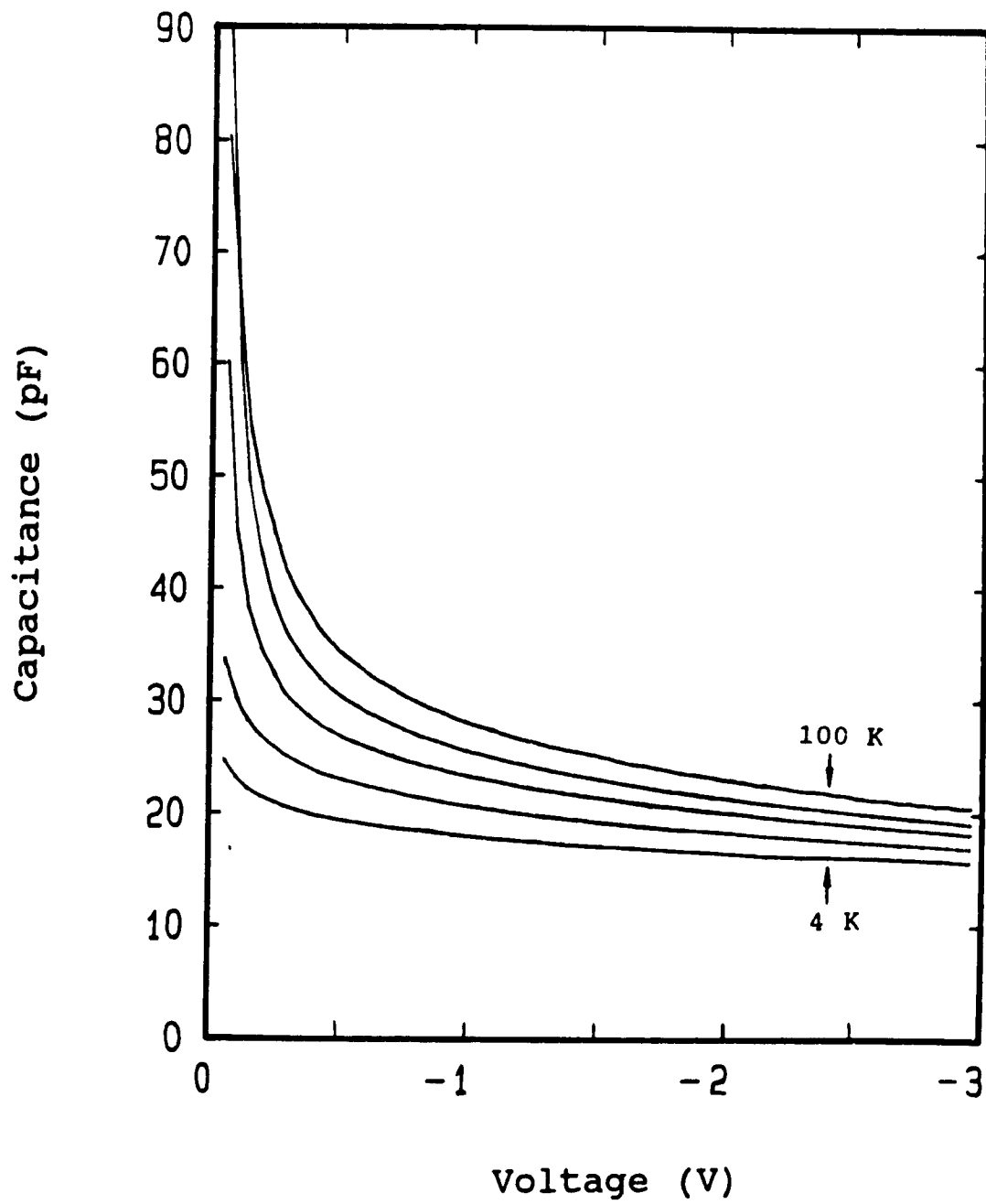


Fig.2.9 Relationship between capacitance and voltage at different measuring frequencies for the sample LH52.

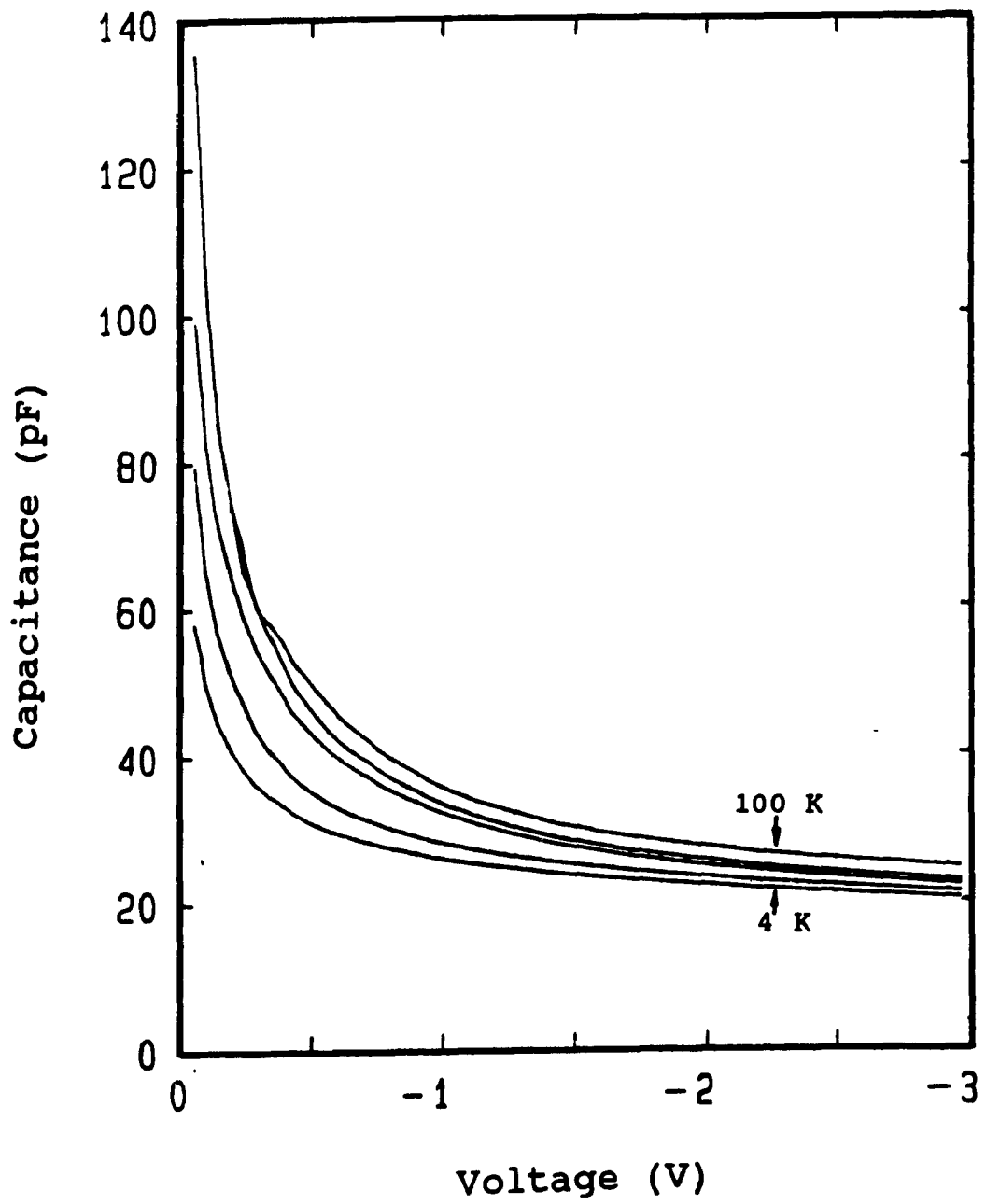


Fig.2.10 Relationship between capacitance and voltage at different measuring frequencies for the sample LH56.

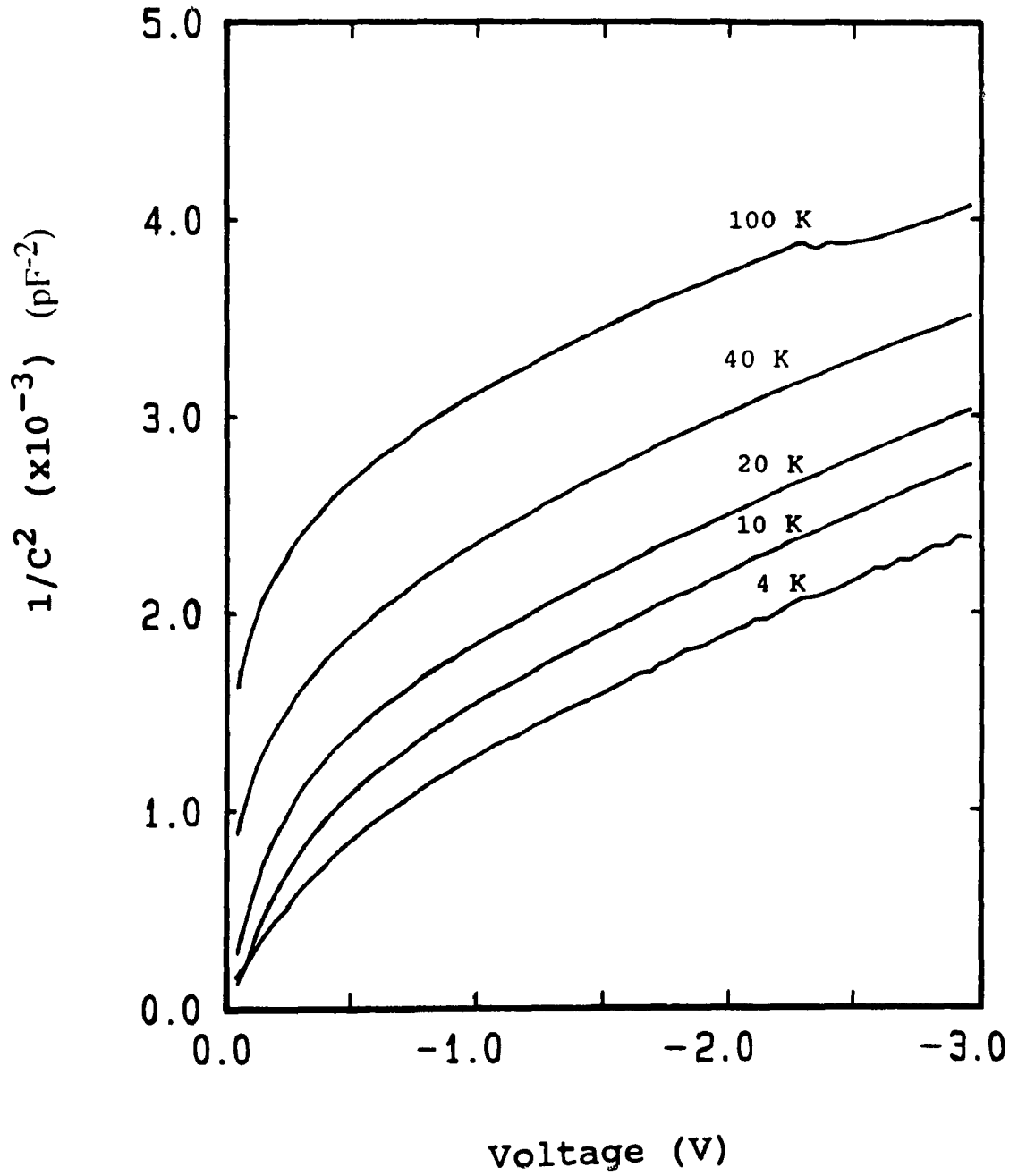


Fig.2.11 Plots of  $1/C^2$  versus V at different measuring frequencies for the sample LH52.

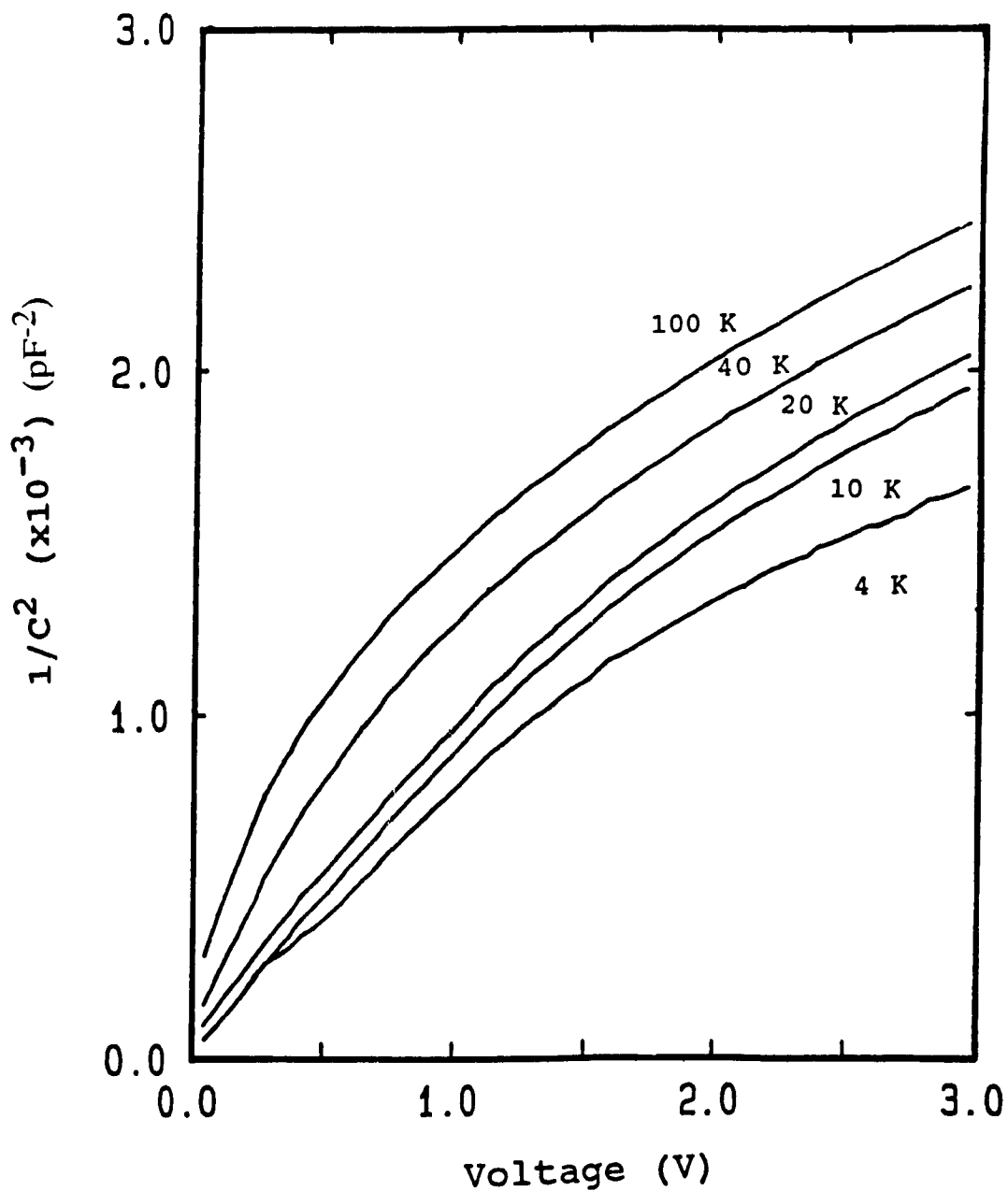


Fig.2.12 Plots of  $1/C^2$  versus  $V$  at different measuring frequencies for the sample LH56.

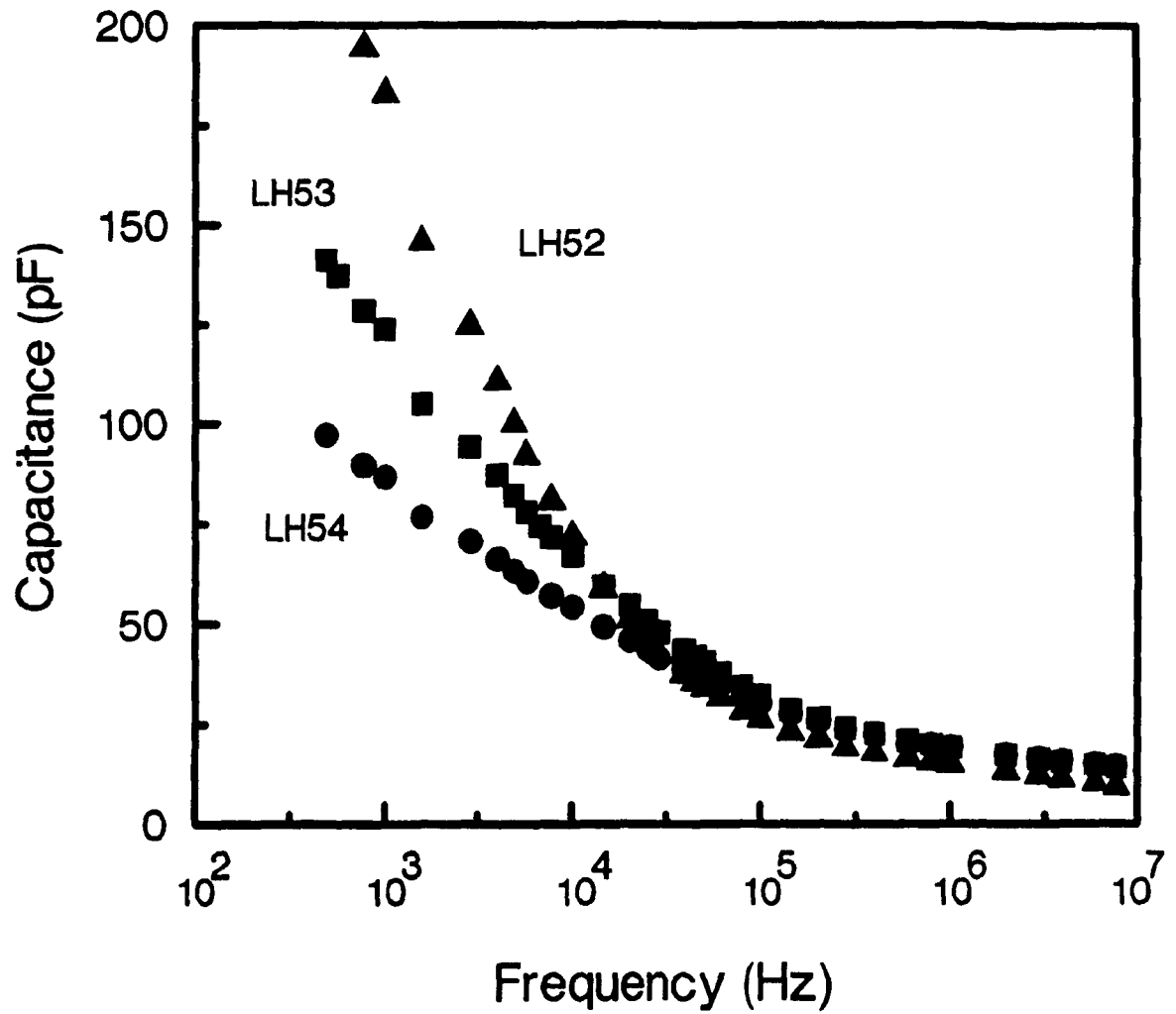


Fig.2.13 Relationship between capacitance and frequency at a fixed reverse bias ( 3 V ) for the samples LH52, LH53 and LH54.

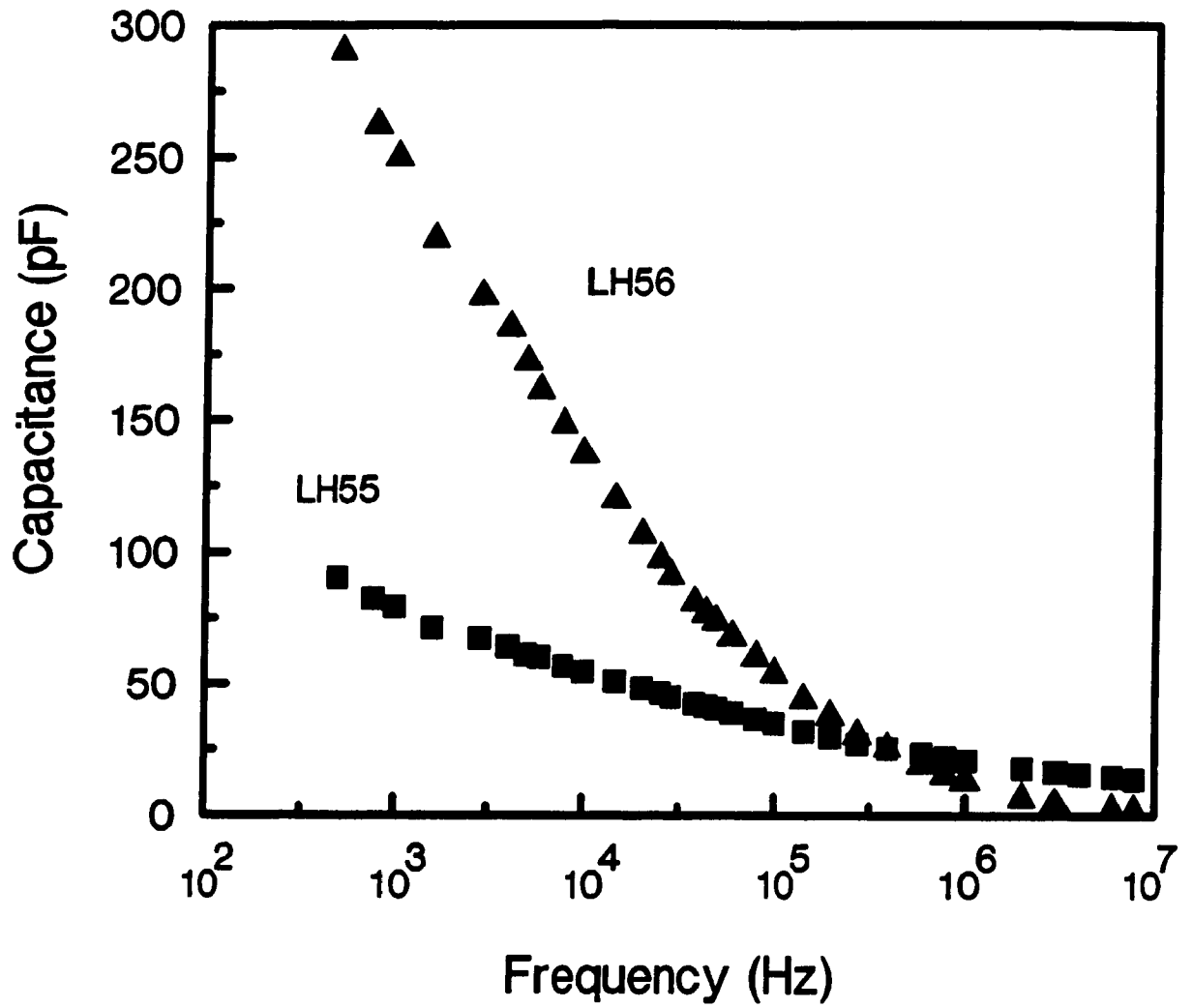


Fig.2.14 Relationship between capacitance and frequency at a fixed reverse bias ( 3 V ) for the samples LH55 and LH56.

## Chapter 3 Principle and System for DLTS Measurements

### 3.1 Principle of DLTS Measurements

#### 3.1.1 The Concept of Deep Levels

Deep levels, which are often called traps or deep defect states, seem to be present in all known semiconductors. The origin of deep levels is often quite complex and these are mainly due to impurities and imperfection in materials. For example, they may be due to large foreign atoms positioned substitutionally or interstitially in the lattice and may be due to vacancies. Sometime they may be caused by host atoms located at wrong lattice sites in compound semiconductors. Deep levels are different from shallow levels and recombination centers. The distinction between deep and shallow levels is the energy position in the band gap. Deep levels often lie far from their related band edges and act at room temperature more stable than shallow levels, which are readily thermally ionized and responsible for electrical conductivity. The difference in definition between deep levels (traps) and recombination centers often depends on the temperature. Generally, carrier

capture rates are used as a criterion. If a defect state has the electron capture rate ( $c_n$ ) as large as the hole capture rate ( $c_p$ ), the defect state is called a recombination center. Consequently, a deep level for the electron trap should have the electron capture rate larger than the hole capture rate ( $c_n > c_p$ ). Similarly, a deep level for the hole trap should have the hole capture rate larger than the electron capture rate ( $c_p > c_n$ ).

On the other hand, electron trap levels are defined as states which become more positively charged when emitting electrons and called donor levels. Hole trap levels can be called acceptor levels which become more negatively charged when emitting holes. Majority carrier traps and minority carrier traps are the other titles for deep levels. In an n-type semiconductor material, the electron traps are designated as majority carrier traps and the hole traps are defined as minority carrier traps. Conversely, the electron traps are called minority carrier traps and the hole traps are majority carrier traps in a p-type semiconductor material.

### 3.1.2 Capture Rate and Emission Rate

Capture rate describes the ability of a trap to capture an electron or a hole. Emission rate determines the degree of a trap to emit an electron or a hole. The thermal capture and

emission mechanisms are illustrated in Fig. 3.1, where  $c_n$  and  $c_p$  are capture rates of electrons and holes,  $e_n$  and  $e_p$  are emission rates of electrons and holes. It should be noted that the capture rates ( $c_n, c_p$ ) should be the summation of the capture rates for radiative and nonradiative capturing processes. In addition to the thermal emission rate, the optical emission rate is also a part of the emission rate. That is:

$$c_{n,p} = c_{n,p}^o + c_{n,p}^i \quad 3.1$$

$$e_{n,p} = e_{n,p}^o + e_{n,p}^i \quad 3.2$$

In this thesis, since all of the experiments were done under a dark condition,  $c_{n,p}^o$  and  $e_{n,p}^o$  can be neglected. So, the capture rates and the emission rates mentioned here are referred to the thermal processes.

The capture rates are related to the capture cross section and the thermal velocity of electrons or holes through the following equation:

$$c_{n,p} = \sigma_{n,p} \cdot V_{n,p} \quad 3.3$$

where  $\sigma_{n,p}$  is the electron (hole) capture cross section,  $V_{n,p}$  is the average thermal velocity of the electron (hole) which can be expressed as:

$$V_{n,p} = \sqrt{\frac{3KT}{m_{e,p}^*}} \quad 3.4$$

Where  $m_{e,p}^*$  is the electron (hole) effective mass, T is the absolute temperature and K is the Boltzmann's constant. It is clear from Eqn. 3.3 that a given defect center, with a specific value of  $\sigma_n$  or  $\sigma_p$ , might be either a trap level or a recombination center, depending on the temperature.

From the detailed balance relationship [3.1], the thermal emission rate omitting the degeneracy of levels can be defined as:

$$e_n = \sigma_n V_n N_C \exp\left(\frac{E_T - E_C}{KT}\right) \quad 3.5$$

$$e_p = \sigma_p V_p N_V \exp\left(\frac{E_V - E_T}{KT}\right) \quad 3.6$$

where  $N_C$  is the effective density of states in the conduction band,  $N_V$  is the effective density of states in the valence band,  $E_T$ ,  $E_C$  and  $E_V$  are the defect state energy, the conduction band and the valence band energies, respectively.

### 3.1.3 Deep Level Parameters and Capacitance Transient

Normally, there are three main parameters for describing the characteristics of deep levels, the activation energy  $\Delta E$ , the trap density  $N_T$  and the capture cross section  $\sigma$ . The activation energy  $\Delta E$  is the energy of traps from the band edge to which the carriers are emitted. It represents the energy difference between the deep levels and the valence band edge for hole traps ( $\Delta E = E_T - E_V$ ). However, it is the energy from the conduction band edge to deep levels for electron traps ( $\Delta E = E_C - E_T$ ). The trap density gives the number of defects existing in the semiconductors and the capture cross sections are related to the properties of traps. These parameters can be determined by a capacitance transient technique on a Schottky barrier or a p-n junction. The transient technique is based on two conditions, one is the initial nonequilibrium condition and the other is the thermal equilibrium of the occupation of the level following the initial condition. From the capacitance transient, one can obtain the activation energy for the deep levels by measuring the time constant as a function of temperature. The initial magnitude of the transient is related to the concentration of the traps. The following description will detail: first, the capture and emission process, and second the capacitance transient expression.

Consider a  $p^+ - n$  junction in the reverse bias condition,

according to the rate equation, the density of trapped electrons  $n_t$  can be depicted as:

$$\frac{dn_t}{dt} = c_n n (N_T - n_t) - e_n n_t - c_p p n_t + e_p (N_T - n_t) \quad 3.7$$

where  $n$  and  $p$  are carrier concentrations.

(a) The capture process is dominant.

For the n-type material, hole concentration is near to zero, and  $e_n \gg e_p$ . So the Eqn. 3.7 is simplified as:

$$\frac{dn_t}{dt} = c_n n (N_T - n_t) - e_n n_t \quad 3.8$$

If the capture process is dominant,  $c_n n \gg e_n$ , and assuming no electrons is captured at  $t=0$ , i.e.  $n_t|_{t=0}=0$ . Then the solution of Eqn. 3.8 is

$$n_t = N_T (1 - \exp(-c_n n t)) \quad 3.9$$

Equation 3.9 presents the electron capture process into initially empty electron traps.

(b) The emission process is dominant.

The Eqn. 3.7 can be written as follows if  $e_n \gg c_n n$ .

$$\frac{dn_t}{dt} = -e_n n_t + e_p (N_T - n_t) \quad 3.10$$

Considering  $e_n \gg e_p$  in the n-type material and assuming the traps are completely filled with electrons at  $t=0$ , that is  $n_t|_{t=0} = N_T$ , the solution of Eqn. 3.10 becomes

$$n_t = N_T \exp(-e_n t) \quad 3.11$$

We defined the time constant ( $\tau$ ) of the emission process to be  $\tau = 1/e_n$ , then

$$n_t = N_T \exp\left(-\frac{t}{\tau}\right) \quad 3.12$$

Eqn. 3.12 describes the electron emission process from initially filled electron traps.

Also considering a  $p^+-n$  junction, the depletion capacitance without traps at a reverse bias  $V_R$  is

$$C = \left( \frac{q\epsilon N_S}{2(V_D + V_R)} \right)^{\frac{1}{2}} A \quad 3.13$$

Where  $N_S$  is the sum of dopant concentrations ( $N_D - N_A$ ),  $V_D$  is the built-in potential,  $\epsilon$  is the permittivity and  $A$  is the

junction area. If there exist a single donor trap level which are completely filled before applying reverse bias, after employing the reverse bias, the carriers emit at a rate given by Eqn. 3.12. The junction capacitance is then changed corresponding to the emission of carriers from the traps.

$$C(t) = \left( \frac{qe(N_S - N_T \exp(-t/\tau))}{2(V_D + V_R)} \right)^{\frac{1}{2}} \cdot A \quad 3.14$$

If the trap density is much smaller than the dopant concentration ( $N_T \ll N_S$ ), using Taylor's series, the Eqn. 3.14 becomes

$$C(t) = \left( \frac{qeN_S}{2(V_D + V_R)} \right)^{\frac{1}{2}} \left( 1 - \frac{N_T}{2N_S} \exp(-t/\tau) \right) \cdot A \quad 3.15$$

At  $t=0$

$$C(0) = \left( \frac{qeN_S}{2(V_D + V_R)} \right)^{\frac{1}{2}} \left( 1 - \frac{N_T}{2N_S} \right) \cdot A \quad 3.16$$

Under a steady-state condition,  $t=\infty$

$$C(\infty) = \left( \frac{qeN_S}{2(V_D + V_R)} \right)^{\frac{1}{2}} \cdot A \quad 3.17$$

Subtracting Eqn. 3.17 from Eqn. 3.15, the capacitance transient given in the following expression is obtained.

$$\begin{aligned}\Delta C(t) &= C(t) - C(\infty) \\ &= \left( \frac{qeN_s}{2(V_D + V_R)} \right)^{\frac{1}{2}} \left( -\frac{N_T}{2N_s} \right) \exp(-t/\tau) \cdot A\end{aligned}\quad 3.18$$

When only a single acceptor trap level exist in the material, the derivation of the capacitance transient is the same as the one described above, except that the bulk concentration is taken as  $N_S - N_T$  and the trap density  $N_T e^{-t/\tau}$  should be added to the bulk concentration in the Eqn. 3.14.

Fig. 3.2 sketches the capacitance transients for majority and minority carrier traps. It is noted that the capacitance transient is an exponential function of time if the density of trap levels is much smaller than the dopant concentration.

At  $t=0$ , the capacitance transient is

$$\Delta C(0) = \left( \frac{qeN_s}{2(V_D + V_R)} \right)^{\frac{1}{2}} \left( -\frac{N_T}{2N_s} \right) \cdot A\quad 3.19$$

The ratio of Eqn. 3.19 and Eqn. 3.17 gives the trap density.

$$\left| \frac{\Delta C(0)}{C(\infty)} \right| = \frac{N_T}{2N_s}\quad 3.20$$

Consequently, the trap density can be obtained directly from the capacitance transient measurements.

### 3.1.4 DLTS Technique

The DLTS is a method based on capacitance transient measurements. It uses a "rate window" to display the time constant of the decaying output signals. The rate window is the inverse of the time interval for the sampling of transient capacitance. If the time constant of the transient decay under investigation is near to the inverse of rate window, a large capacitance difference can be detected. The variation of the capacitance difference with temperature is called a DLTS spectrum.

The procedure of DLTS measurements can be simply explained using a one-sided junction. First of all, a reverse bias  $V_R$  is applied to the junction. A fill pulse with a certain duration is then applied to fill all traps in the depletion region. Generally, there are two types of fill pulses: the majority carrier pulse which has an amplitude  $V_F \leq 0$  and the injection pulse with magnitude  $V_F$  larger than zero. The majority carrier pulse reduces momentarily the diode bias and introduces only majority carriers into the depletion region. However, the injection pulse drives the diode into forward bias and injects minority carriers into the region to be investigated. Fig. 3.3 shows the operating processes of the two pulses. After filling

all of the traps, the junction bias is reduced to the original value  $V_R$ . At this time, the depletion region reaches a new position because of the existence of the trapped states. The trapped states begin to release their trapped charges at an emission rate given in Eqn. 3.5 or Eqn. 3.6. The depletion region is then changed corresponding to the trap emission from the new position to the original position. The capacitance transient is thus resulted during the trap emission period as given in Eqn. 3.18.

The usual method for measuring the capacitance transient is the boxcar technique. Here the capacitance transient is sampled twice at time  $t_1$  and  $t_2$ . The inverse of time period between the sampling points is referred to as the rate window. The shape of the transient is a function of the temperature. At a certain temperature, when the emission rate is matched to the rate window, a maximum  $\Delta C(C(t_2) - C(t_1))$  will be obtained. Fig. 3.4 illustrates the variation of capacitance transient with temperature. The curve in the right hand side of the Fig. 3.4 is the DLTS spectrum.

The normalized DLTS signal,  $S(T)$ , can be defined as

$$S(T) = \frac{C(t_2) - C(t_1)}{\Delta C(0)} \quad 3.21$$

Where  $\Delta C(0)$  is the capacitance change due to the fill pulse

at  $t=0$  as shown in Eqn. 3.19. From Eqn. 3.15 and Eqn. 3.19, the normalized DLTS signal can be simplified as

$$S(T) = \exp(-t_2/\tau) - \exp(-t_1/\tau) \quad 3.22$$

Where the temperature dependence of  $\tau$  is given by the Eqn. 3.5 and the Eqn. 3.6 with  $\tau = 1/e_{n,p}$ . At the peak of the DLTS spectrum, we should have

$$\left. \frac{dS(T)}{d\tau} \right|_{\tau=\tau_{\max}} = 0 \quad 3.23$$

Taking the derivative of the Eqn. 3.23

$$e_{\max} = \frac{1}{\tau_{\max}} = \frac{\ln(t_2/t_1)}{t_2 - t_1} \quad 3.24$$

Thus, the emission rate at the maximum of a DLTS spectrum is specified and is equal to the rate window value set in the DLTS system.

In order to derive the activation energy, Eqn. 3.5 (or the Eqn. 3.6) is used. It is noted that the temperature dependence of  $\sigma$  is neglected and  $\sigma V_n N_C$  is proportional to the temperature square,  $T^2$ . So, the emission rate has the following temperature dependence relation,

$$e_n = \text{const.} \cdot T^2 \exp\left(\frac{\Delta E}{KT}\right) \quad 3.25$$

At the peak of the DLTS spectrum, Eqn. 3.25 becomes

$$e_{n,\text{max}} = \text{const.} \cdot T_{\text{max}}^2 \exp\left(\frac{\Delta E}{KT}\right) \quad 3.26$$

If an Arrhenius plot of  $\ln(e_{n,\text{max}}/T_{\text{max}}^2)$  versus  $1/T_{\text{max}}$  is made, the slope of the plot will give the activation energy of traps,  $\Delta E$ .

The determination of deep level density using the DLTS system is based on Eqn. 3.20

$$N_T = \frac{2\Delta C(0)}{C} \cdot N_S$$

Where  $N_S$  is the net doping concentration in the semiconductor,  $C$  is the steady-state capacitance under the reverse bias  $V_R$  and  $\Delta C(0)$  is the magnitude of capacitance transient at  $t=0$ .

The capture cross section can be obtained by several methods. The simplest one is based on the determination of the intercept of the Arrhenius plot. However, this is often not accurate because of the temperature dependence of the capture

cross section. The value of the capture cross section obtained using this method corresponds to the value at  $T=\infty$ . In the DLTS technique, the capture cross section is determined using an injection or majority carrier pulse with different pulse durations. Assuming there are no carriers trapped initially in a donor trap level, the number of captured carriers given by Eqn. 3.9 will increase with the increase of the pulse duration,  $t$ . Using Eqn. 3.9 and Eqn. 3.13 and assuming that the trap density is much smaller than the dopant concentration ( $N_T \ll N_S$ ), the junction capacitance during the capturing process is given by,

$$C(t) = \left( \frac{qe(N_S - N_T)}{2(V_D + V_R)} \right)^{\frac{1}{2}} \left( 1 + \frac{N_T}{2(N_S - N_T)} \exp(-c_n n t) \right) \cdot A \quad 3.27$$

Where the parameters have the same meaning as before except for  $t$ , which is defined as the fill pulse duration.

If the pulse duration is long enough, all traps are filled during the fill pulse period. The junction capacitance becomes

$$C(t_{sat}) = \left( \frac{qe(N_S - N_T)}{2(V_D + V_R)} \right)^{\frac{1}{2}} \cdot A \quad 3.28$$

Defining  $f = [C(t) - C(0)] / [C(t_{sat}) - C(0)]$ , which is also equal to the ratio of the peak value for a given pulse duration and the saturation peak value, we have

$$1-f = \exp(-c_n n t) \quad 3.29$$

If we define  $\tau = 1/c_n n$ , which is the time constant for the capture process, then  $\tau$  can be obtained from the slope of a  $\ln(1-f)$  versus  $t$  plot. According to Eqn. 3.3, the capture cross section can be calculated from:

$$\sigma_n = \frac{1}{\tau n V_{th}} \quad 3.30$$

It should be noted that the majority carrier capture cross section is readily obtained from Eqn. 3.30 because the majority carrier concentration can be easily measured. However, for the minority carrier capture cross section, it becomes quite complicated since the minority carrier concentration depends on the injection mechanism [3.2] [3.3].

The DLTS technique has many advantages over other techniques for detecting defects in semiconductors. It is sensitive and convenient for practical applications even though some limitations have been reported by other investigators. For example, the leakage current of a device should be small enough, otherwise an error in the DLTS peaks will occur [3.4]. In addition, minority carrier emission effect can not be neglected if the detected level has a large activation energy [3.5]. Moreover, a Schottky diode or a one-sided junction may

be the better device for investigating the material defects. Conventional p-n junction should be avoided since information obtained from the DLTS measurements always contains two parts, both n-type side and p-type side.

### 3.2 DLTS System

The DLTS system used in the present experiments is a Polaron model S4600 DLTS system. It consists of six main parts: a capacitance meter, a pulse excitation unit, a signal processor, a sample cryostat, a temperature controller and a data recording unit. A block diagram of the measurement system is shown in Fig. 3.5.

#### 3.2.1 Capacitance Meter

The Boonton model 72B capacitance meter is the most important part of the S4600 DLTS system. Apart from making quantitative C-V and C-T measurements, the meter is designed to allow fast rate window transient measurements (up to  $2000 \text{ s}^{-1}$ ). The signal output of the meter is connected to the signal processing unit by an interface unit. The pulse excitation system applies a pulse bias to the meter by a capacitance offset unit.

### **3.2.2 Pulse Excitation Unit**

This unit provides all of the bias pulses required for the DLTS measurements, controls the timing, collects and processes the DLTS data.

The pulse excitation unit contains a power supply, a pulse generator, a pulse timer, a master clock and an IEEE-488 interface. The power supply controls the pulse amplitudes applied to the sample. The pulse generator provides various pulse sequences which are needed for different DLTS operation modes. It also controls the widths of fill and clear pulses. The pulse timer has a high resolution and can precisely measure the period of the DLTS pulse repetition and the widths of fill and clear pulses. The master clock has a function of controlling the timing for the entire pulse excitation system. It is used to generate the appropriate timing and duration of the sampling pulses for the signal processor. Finally, the IEEE-488 interface connects the DLTS system to a computer.

### **3.2.3 Signal Processor**

The signal processor is the most critical component of the DLTS system. The module takes the output from the capacitance meter and applies to the signal processor. The timing requirements for this unit are supplied by the master clock module.

The signal processor can be thought of as a triple boxcar unit in which three samples of the input signal are collected at time  $t_1$ ,  $t_2$  and  $t_3$  respectively. Fig. 3.6 illustrates the process schematically by giving a capacitance transient and the corresponding pulse sampling times. Two DLTS signals are obtained in one process in the present system. The Polaron model S4650 signal processor accepts a sampling pulse width which matches the rate window so that it remains short compared to the transient time constant as the DLTS peak is swept. However, the pulse width is long compared to a typical commercial boxcar sampling pulse. This permits averaging during the sampling time and improving the signal to noise ratio.

#### 3.2.4 Cryostat and Temperature Controller

The cryostat is an important part of the DLTS system. Fig. 3.7 shows a schematic diagram of the cryostat. The sample is mounted in a copper stage and liquid nitrogen is pumped into the cryostat from a large dewar. The heater is connected to the underside of the sample stage. Between the heater and the stage, a thin layer of thermally conducting grease is applied to improve the thermal contact. A vacuum system is used to evacuate the cryostat. At top of the cryostat, a circular window is furnished for optical measurements.

A three action controller is used to control the tempera-

ture in the DLTS system and a microprocessor is employed to manage the temperature ramp function. In addition to controlling the heater output, the controller determines the liquid nitrogen pumping speed. The lower the required sample temperature is, the higher the pumping speed is used.

### **3.2.5 Data Recording Unit**

The data obtained from the DLTS measurements is managed by a Hewlett Packard computer (model HP9816). The computer uses the IEEE-488 bus for device control and data acquisition. All of the DLTS measurements can be managed and recorded under software control after the measurement conditions have been established.

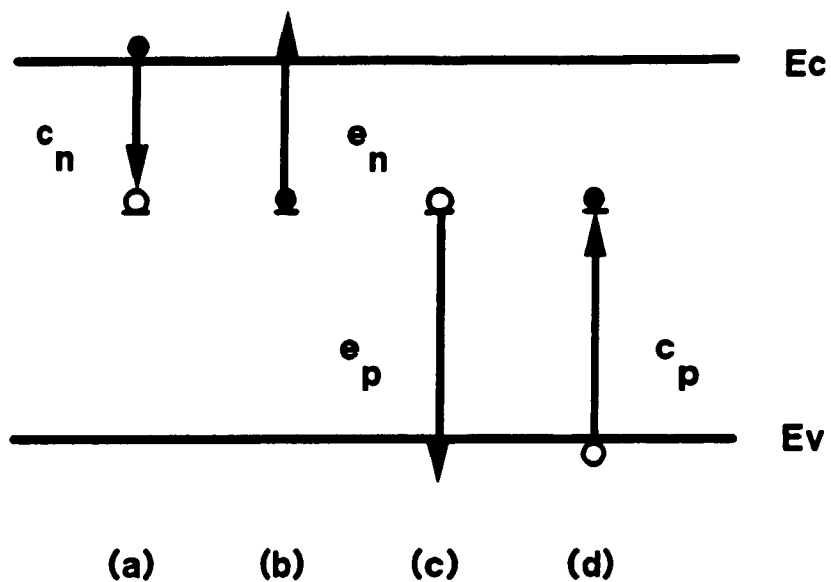


Fig.3.1 Thermal emission and capture processes of electrons and holes at deep-level defects. (a) electron capture, (b) electron emission, (c) hole emission, (d) hole capture.

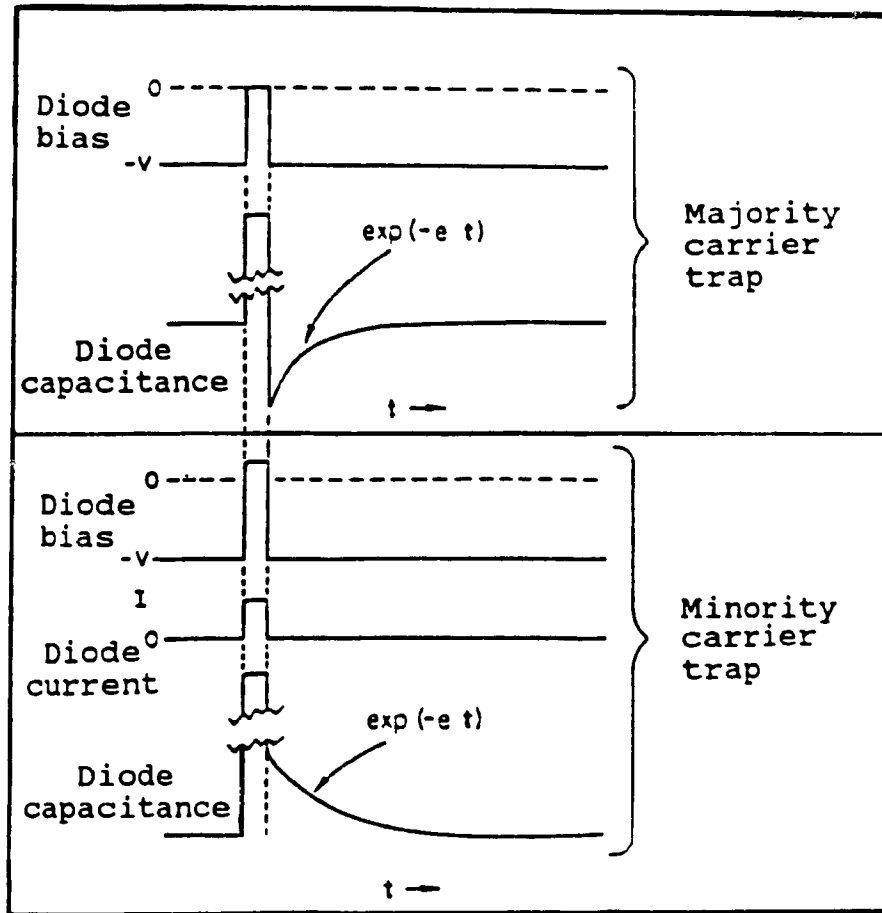


Fig.3.2 Capacitance transients for majority and minority carrier traps.

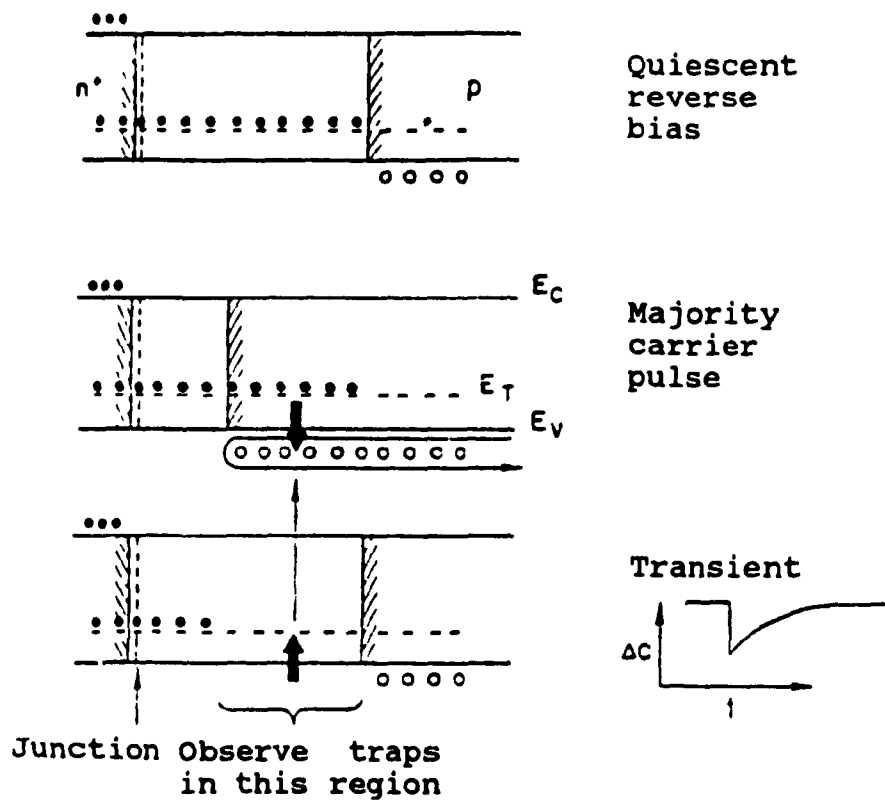


Fig.3.3(a) Operating process for the majority carrier pulse.

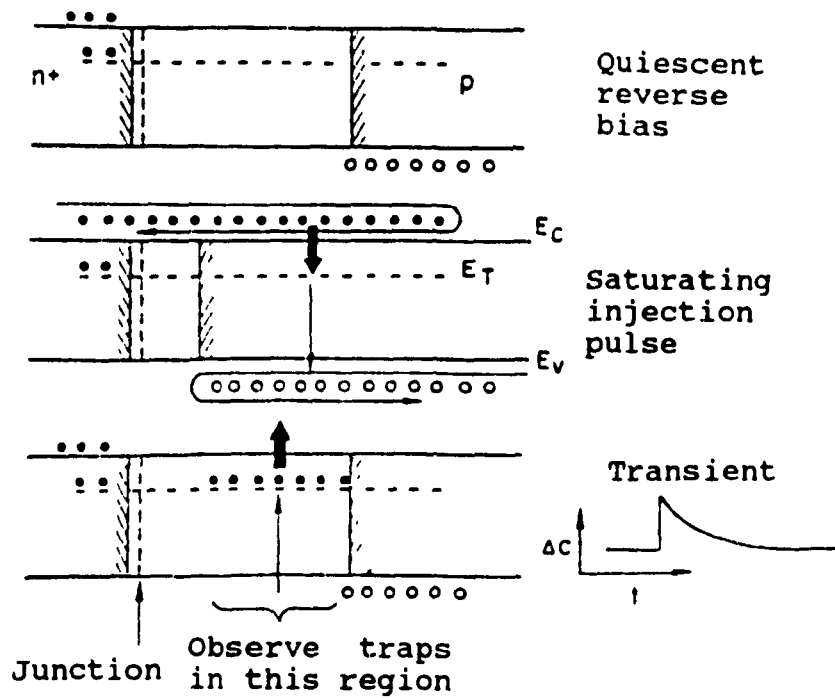


Fig.3.3(b) Operating process for the injection pulse.

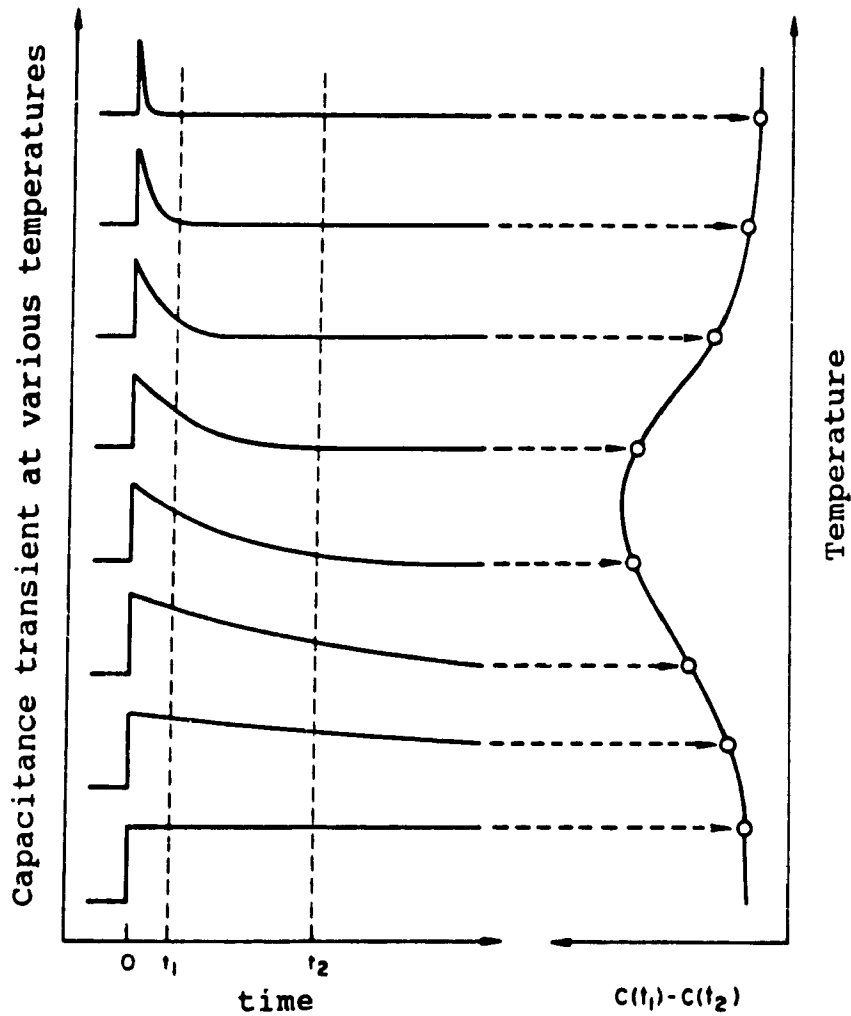


Fig.3.4 Implementation of a rate window by means of a double-boxcar integrator. The output corresponds to the (average) difference of the amplitudes at the sampling times  $t_1$  and  $t_2$ .

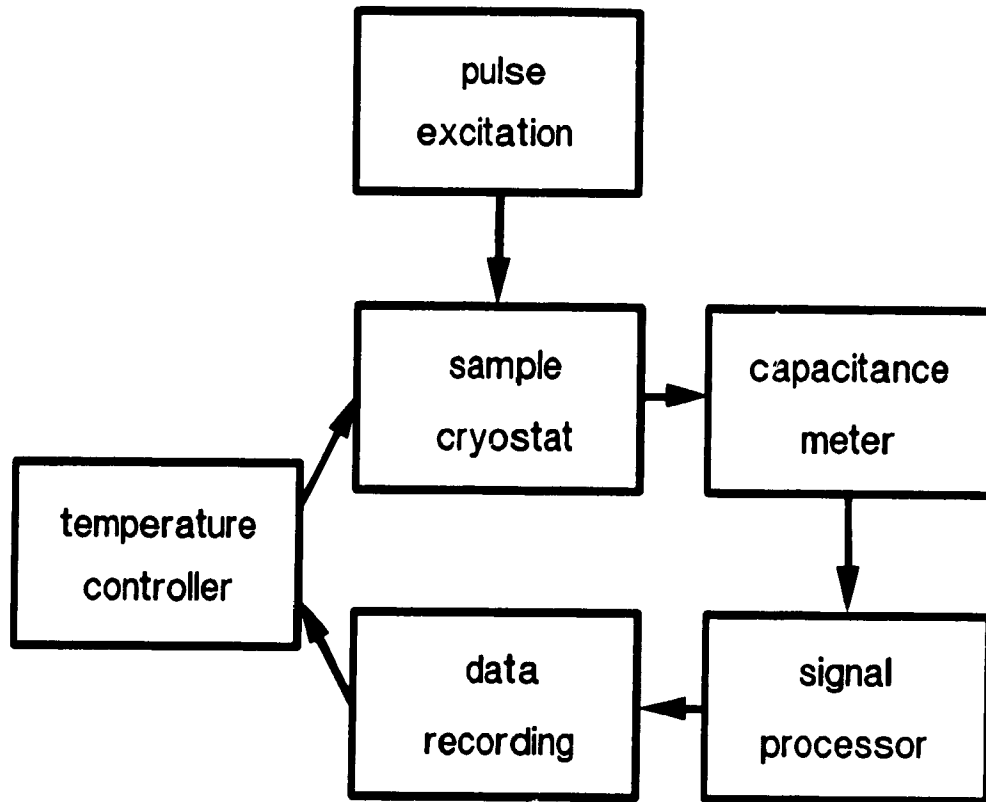


Fig.3.5 A block diagram of the DLTS system

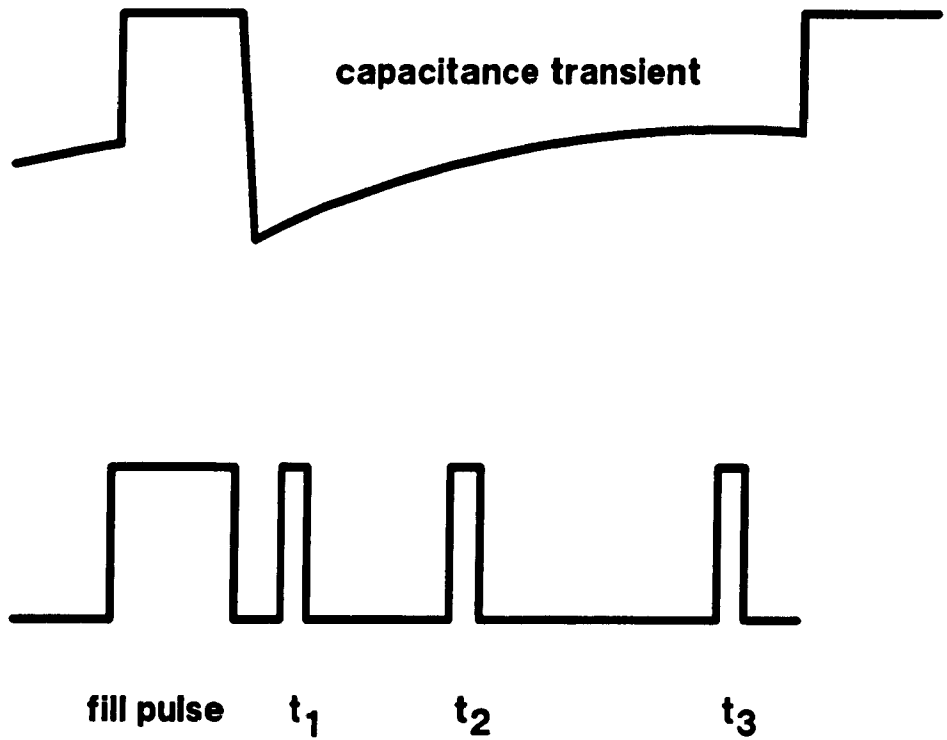


Fig.3.6 Timing pulse output of the Polaron S4650 signal processor for the sampling of the transient capacitance.

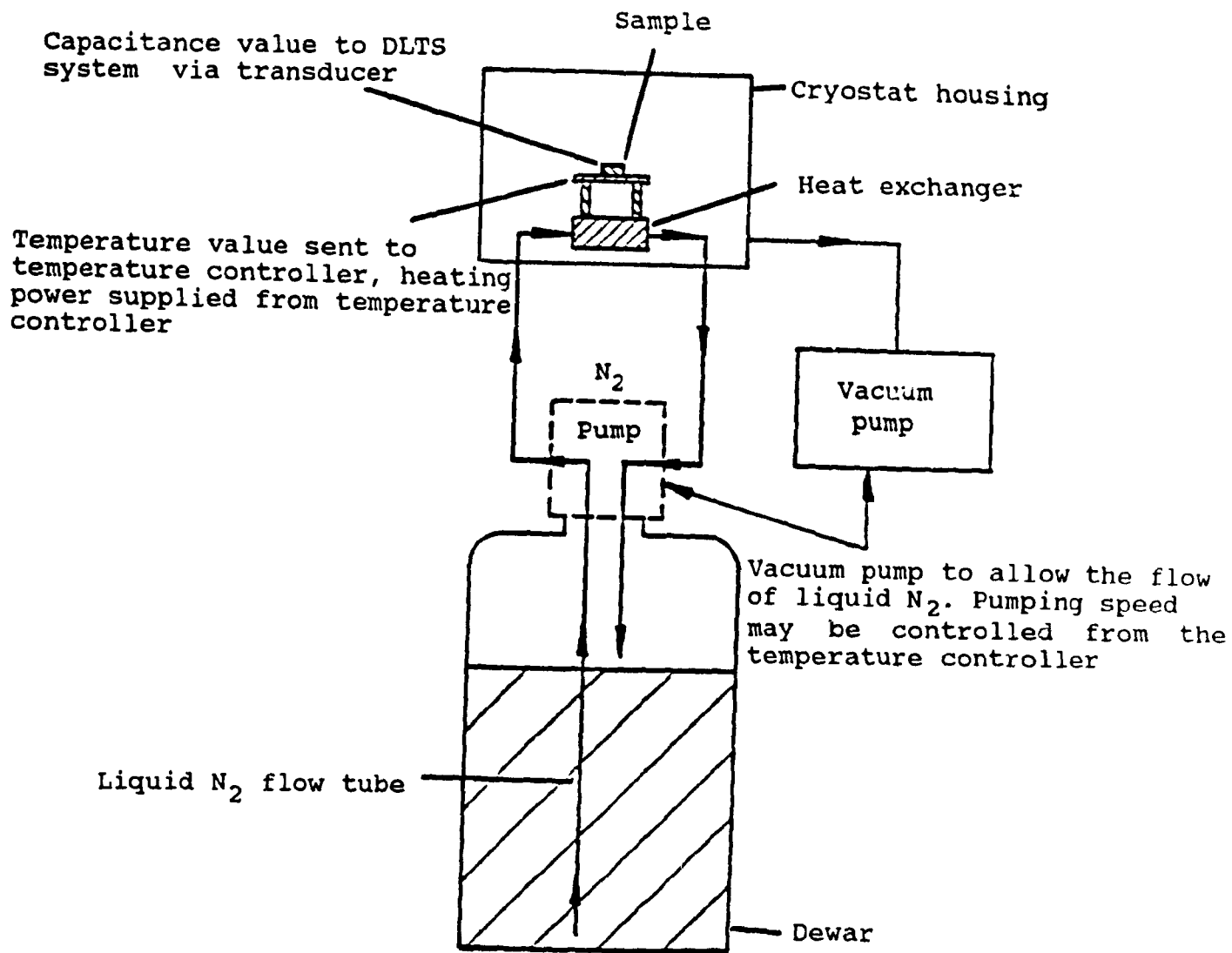


Fig.3.7 A schematic diagram of the cooling unit for the Polaron model S4600 DLTS system.

## Chapter 4 DLTS Measurements on CuInSe<sub>2</sub> Junctions

In order to obtain information on deep levels in the material, DLTS measurements have been carried out on all of the CuInSe<sub>2</sub> homojunctions fabricated on the p-type Bridgman-grown monocrystalline samples. Measurements were separately carried out to determine hole trap levels and electron trap levels. The trap parameters, like activation energy, density and capture cross section, were specifically studied. In this chapter, the measurements on hole traps are first described. Results for electron trap measurements are then presented.

### 4.1 Capacitance Transient for Hole Traps

Before carrying out the DLTS measurements, capacitance transients of all samples were studied. The objectives of the capacitance transient measurements are: [1] to obtain a qualitative information about the traps involved (single or multiple deep levels) and [2] to determine the appropriate parameters for the DLTS system, such as the fill pulse duration and the fill pulse height. The capacitance transients were observed on

a Hewlett Packard model 5450 2A digitizing oscilloscope with a capability of 400 M samples/sec. The capacitance transient obtained from the oscilloscope is the average value with either 512 or 1024 repetitions. The transient data was printed using a printer.

First of all, the capacitance transients were investigated with different fill pulse height. It was found that the capacitance transients were dependent on the magnitude of the fill pulse ( $V_F$ ). When the fill pulse height ( $V_F$ ) was equal to or less than zero volt, which is called a majority carrier pulse, only negative capacitance transients (due to hole traps) were obtained. As the fill pulse height was increased, the absolute value of the negative transient decreased and finally a positive capacitance transient (due to electron traps) appeared. Fig. 4.1 illustrates experimental results of the capacitance transients under three different fill pulse heights at 150 K for the sample LH53. The results confirmed that both hole traps and electron traps are present in monocrystalline  $\text{CuInSe}_2$ . The results in Fig. 4.1 also show that it is critical to select appropriate fill pulses for detecting either the hole traps or the electron traps. A majority pulse ( $V_F \leq 0$ ) is used for observing the hole traps. An injection pulse ( $V_F > 0$ ) with large enough magnitude should be adopted in order to eliminate the effect of the hole traps and detect the electron traps.

During the observation of the capacitance transients due to the hole traps, it was also found that the magnitude of the

capacitance transients was dependent on the fill pulse duration. If the fill pulse duration was too narrow, the hole traps were not completely filled and the corresponding magnitude of the capacitance transient was small. When the fill pulse with a long enough duration was applied, all of the traps captured the holes from the valence band during the pulse period and a maximum capacitance transient was attained. The relationship between the fill pulse duration and the capacitance transient for the sample LH53 at temperatures of 150 K and 300 K is depicted in Fig. 4.2. First, it is noted that the magnitude of capacitance difference at  $t=0$  increases with the increase of temperature. Second, the magnitude increases from 3 msec and then reaches a constant value at about 10 msec as the fill pulse width is increased. The present results thus suggest that the fill pulse with a duration of 10 msec is enough to fill all of the hole traps.

For an ideal single trap level, the capacitance transient is an exponential function of time (see Eqn. 3.18) if the trap density is much smaller than the dopant concentration. The plot of  $\ln\Delta C$  versus time ( $t$ ) should be a straight line with a fixed emission rate. Capacitance transient measurements for the sample LH53 have been made at a reverse bias of 3 V and with a majority fill pulse having a duration of 10 msec. Fig. 4.3 sketches the dependence of  $\ln\Delta C$  on time at 150 K and 300 K. It is seen that the plots are not linear, implying that there is

more than one type of deep level in the material. By assuming two types of deep levels, the time constants were determined to be about 2 msec and 20 msec for the sample LH53 at 300 K.

## 4.2 Hole Trap Parameters

After the capacitance transient measurements described above, DLTS measurements were performed for all of the samples using the Bio-Rad model DL4600 DLTS system with a Boonton model 72B capacitance meter (operating frequency 1 MHz). The temperature range of the measurements was from 80 K to 320 K with the samples located in an evacuated cryostat. The temperature control and data acquisition were achieved using the Hewlett Packard model 9122 microcomputer. The height of the applied fill pulse was equal to zero volt ( $V_F$ ) and the duration was 10 msec. The rate window used in the present experiments was from 50/sec to 1000/sec and the reverse bias was set at 3 volts. Two positive peaks were perceived in all of the samples at two different temperatures. It is thus evident that there are two types of hole traps in the monocrystalline  $\text{CuInSe}_2$  fabricated in our laboratory. Fig. 4.4 gives the DLTS spectra of the samples LH51 and LH53 at a rate window of 80/sec. For the sample LH51, which was treated at 200 °C for 10 minutes in  $\text{N}_2$ , the two peaks overlap and the high temperature one is not very clear. This result implies that these two types of hole traps

have relatively close emission rates. The activation energy values of these traps with the overlapped DLTS peaks can not be determined simply from an Arrhenius plot of the emission rate [4.1]. On the other hand, two positive peaks (one is at 150 K and the other at about 270 K) appear in the same temperature range for the sample LH53 which was treated at 200 °C for 40 minutes in N<sub>2</sub>. In order to estimate the activation energy of the traps, Arrhenius plots ( $\ln(e/T^2)$  versus  $1000/T$ ) for the two peaks were made and the results are shown in Fig. 4.5. The activation energy value for the high temperature peak is 535 meV from the valence band edge and is 263 meV for the low temperature one. DLTS measurements were also carried out on the other samples. From these samples, the average activation energy for the high temperature peaks is  $520 \pm 15$  meV and is  $250 \pm 15$  meV for the low temperature ones. The activation energy of  $250 \pm 15$  meV is very close to the value reported by Fabik and Eskenas [1.23] for polycrystalline CdZnS/CuInSe<sub>2</sub> thin film cells (237 meV). The other trap with the energy value of  $520 \pm 15$  meV is near to one of the trap (498 meV) reported by Hanak et al [1.25] for their CdS/CuInSe<sub>2</sub> cell fabricated using a monocrystalline CuInSe<sub>2</sub> substrate. DLTS spectra similar to that shown in Fig. 4.4 were also observed for the sample LH54, which was treated at 200 °C for 20 minutes in air. From the Arrhenius plots for this sample shown in Fig. 4.5, the activation energy for the low temperature peaks is 236 meV from the valence band edge. However, the activation energy is 850 meV for the high

temperature peaks. The high activation energy seems to be caused by the heat treatment of the sample in an ambient containing oxygen. It should be noted that hole traps located at 800 meV from the valence band edge have been reported previously by Eron and Rothwarf [1.22] on polycrystalline CdZnS/CuInSe<sub>2</sub> thin film solar cells. During the fabrication of the CuInSe<sub>2</sub>-based solar cells, a heat treatment in air is often carried out to form the heterojunctions. This suggests that O atoms may have led to a new deep level in the material or formed a new deep center with the original trap atoms.

There are two methods which can be used to estimate the deep level density. One is based on the magnitude of the capacitance transient at  $t=0$  and the other is on deduction of the data from the DLTS spectra. The density of hole traps obtained from the two methods should be the same if there is only one type of traps in the material and the capacitance transient is pure exponential. From the capacitance transients at  $t=0$ , the value of the hole trap density was estimated to be about  $8 \times 10^{13} \text{ cm}^{-3}$  for the sample LH53. Table 4.1 lists densities of the two kinds of hole traps obtained from the DLTS spectra for all of the CuInSe<sub>2</sub> homojunctions. It is noted that the hole trap densities are in the order of  $10^{13} \text{ cm}^{-3}$ .

The capture cross section of the hole traps with the activation energy of 520 meV has been measured by the DLTS system. The method involves the observation of the variation of height

of DLTS signal with the variation of fill pulse duration. A fast pulse interface unit was attached to the DLTS system to produce fill pulses with smaller durations. Six fill pulse durations, 5 nsec, 10 nsec, 100 nsec, 500 nsec, 2 msec and 20 msec, were chosen. The height of the DLTS signals was observed to increase gradually with the increase of the fill pulse duration and finally reach a constant value. A plot of  $\ln(1-f)$  versus the pulse duration  $t$  ( $f$  is the ratio of the peak height for a given pulse width and the saturated peak height) for the sample LH53 is sketched in FIG. 4.6. It is seen that the plot is not linear with a unique slope. The value of capture cross section derived from the plot is in a range from  $2.2 \times 10^{-19}$  to  $1.2 \times 10^{-18}$   $\text{cm}^2$ . This result may be caused by a non-flat energy bend at a small filling pulse during the measurements or indicates that the hole trap level may have a broad energy distribution.

### 4.3 Capacitance Transient for Electron Traps

Using the same DLTS system and method for hole traps, capacitance transients were investigated in the  $\text{CuInSe}_2$  homojunctions for electron traps. During the investigation of the capacitance transients, an injection pulse was applied and the positive transients were recorded using the HP digitizing oscilloscope. The capacitance transient  $\Delta C(t)$  ( $=C(t)-C(\infty)$ ) was found to be

dependent on the magnitude of injection pulses ( $V_F$ ). As an example, Fig. 4.7 shows the results of  $\Delta C(t)$  versus  $V_F$  at two different temperatures for the sample LH53. Due to the presence of electron traps in the p-type  $\text{CuInSe}_2$ , the capacitance transients  $\Delta C(t)$  at 150 K or 100 K were positive when a 10 msec injection fill pulse with a small magnitude was applied. As the magnitude of the injection pulse was increased gradually to 2 volts, the  $\Delta C(t)$  first increased and then attained a stable value. The reason for this variation is due to the amount of electrons injected into the depletion region, which varies with the pulse height  $V_F$ . Therefore, in order to fill all of traps in the depletion layer and eliminate the effect of hole traps, the height of the injection pulse should be equal to or larger than 2 volts. Accordingly, most of the DLTS measurements for the electron traps in the thesis were performed using a fill pulse with a value of 2.4 volts.

Due to the same reason as that for the hole traps, the capacitance transients are also dependent on the injection pulse width. It has been verified from the measurements of the capacitance transients that a duration of 5 msec is enough to fill all of the electron traps.

In order to study the type and emission rate of the electron traps, plots of  $\ln \Delta C(t)$  versus time  $t$  were made using the data taken from the capacitance transient measurements. The results of the sample LH53 are displayed in Fig. 4.8. It is seen that the plots are almost linear at three different tem-

peratures. This result demonstrates that the electron traps in the monocrystalline p-type  $\text{CuInSe}_2$  are a single level. The time constants of emission process calculated from the plots are 0.37 msec, 20 msec and 38 msec for 200 K, 150 K and 100 K respectively.

#### 4.4 Electron Trap Parameters

The DLTS measurements for electron traps were performed on all of the samples. In such experiments, an injection pulse with a height of 2.4 V was used. The pulse duration was set at 10 msec and the temperature range was from 100 K to 300 K. The DLTS spectra of the samples LH53 and LH54 are illustrated in Fig. 4.9. Spectra for the samples LH55 and LH56 are presented in Fig. 4.10. These results were obtained at a rate window of 200/sec and a reverse bias of 3 V. It is seen that the peaks of DLTS spectra are located at temperatures near to 160 K for the samples LH53, LH54 and LH55. However, it is noted that the peak position is at about 140 K for the sample LH56, and another small peak appears at a relatively high temperature. The Arrhenius plots for the samples LH54 and LH55 are shown in Fig. 4.11 yielding an activation energy of 183 meV below the conduction band edge for the sample LH54 and 185 meV for the sample LH55. The electron trap density was also estimated from the capacitance transients at  $t=0$  and the DLTS spectra. Table 4.2 shows

the data of the activation energy  $\Delta E$ , the trap density  $N_T$  and the width at half height of the DLTS spectrum for all of the samples. From these results, an electron trap level is ascertained to be located at  $182 \pm 14$  meV from the conduction band edge and the average trap density is  $6.4 \times 10^{14} \text{ cm}^{-3}$ . This electron trap level is very similar to the one reported by Irie, Endo and Kimura using electrical measurements on n-type monocrystalline samples [1.29].

Since it is more difficult to determine the injected electron densities in  $\text{CuInSe}_2$  during the DLTS measurements, the capture cross sections of the electron traps are only calculated at  $T = \infty$ . (which are derived from the intercept of the Arrhenius plot.) The value of the capture cross section of electron traps is  $1.58 \times 10^{-17} \text{ cm}^2$  for the sample LH52. To obtain more accurate values of the electron capture cross sections and understand their dependence on temperatures, the injected electron densities should be calculated from the injected currents [3.3] or a Schottky junction with an n-type  $\text{CuInSe}_2$  substrate should be fabricated for the DLTS measurements. Furthermore, the properties of electron traps can also be studied using the DLTS system with a laser excitation unit.

To understand the electron trap distribution in the material, the trap density profile was also investigated by carrying out DLTS measurements at different reverse bias voltages and at a given rate window. The measurements were controlled by the

computer and twelve reverse biases ranging from 0.2 V to 4.2 V were applied. The temperature range used was from 135 K to 185 K since the DLTS peaks for the electron traps were located near 160 K. Fig. 4.12 shows the DLTS spectra at different reverse biases for the sample LH53. It is noticed that the peak height increases when the magnitude of the reverse bias voltage is decreased. The trap density profile was then calculated by the computer using the data in Fig. 4.12 and the results are given in Fig. 4.13. It is seen that the trap density near the surface appears to be greater than that far from the surface. The reason for this is still not clear. It may be caused by the diffusion process or contamination from the ambient. Alternatively, it may be due to the fixed substrate doping concentration, which was taken at a large reverse voltage, supplied to the computer before the calculation. This fixed concentration is greater than the actual doping concentration in the region near the surface (as evident from Fig. 2.11 ), causing the calculated trap density to be greater than the actual value.

Table 4.1 Densities of hole traps for all of the CuInSe<sub>2</sub> homojunctions studied in the present work.

Sample No.	V <sub>R</sub> (V)	Trap Density (cm <sup>-3</sup> )	
		Low Temperature Peaks (rate window: 1000/s)	High Temperature Peaks (rate window: 400/s)
LH51	3.9	1.45x10 <sup>13</sup>	
LH52	2.5	1.52x10 <sup>13</sup>	2.12x10 <sup>13</sup>
LH53	3.5	1.3x10 <sup>13</sup>	1x10 <sup>13</sup>
LH54	3.6	1.25x10 <sup>13</sup>	4x10 <sup>12</sup>
LH55	3.0	2.5x10 <sup>13</sup>	1.25x10 <sup>13</sup>
LH56	3.0	9.5x10 <sup>12</sup>	1.6x10 <sup>13</sup>

Table 4.2 Electron trap energy level, trap density, peak width at half height and diffusion source for all of samples.

Sample No.	Energy Level* (meV)	Trap Density (cm <sup>-3</sup> )	Peak Width at Half Height (K)	Diffusion Source
LH11A	168	1.1x10 <sup>14</sup>	34	In
LH52	197	3.0x10 <sup>14</sup>	33	In
LH53	175	1.5x10 <sup>15</sup>	36	In
LH54	183	1.3x10 <sup>15</sup>	46	In
LH55	185	5.0x10 <sup>14</sup>	50	Bi
LH56	186	1.5x10 <sup>14</sup>	32	Bi

\* From the conduction band edge.

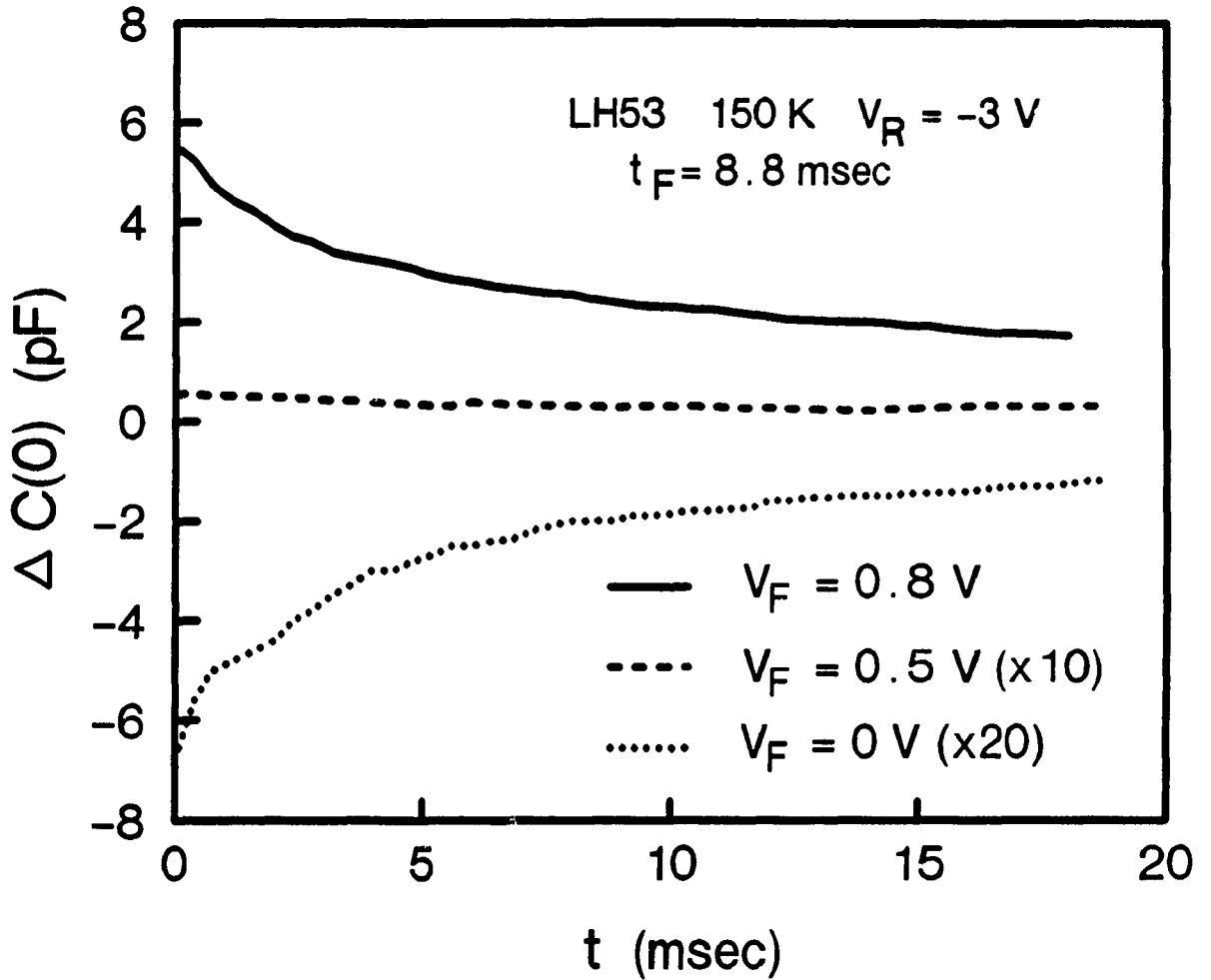


Fig.4.1 Plots of transient capacitance with time showing the variation with the fill pulse height for the sample LH53.

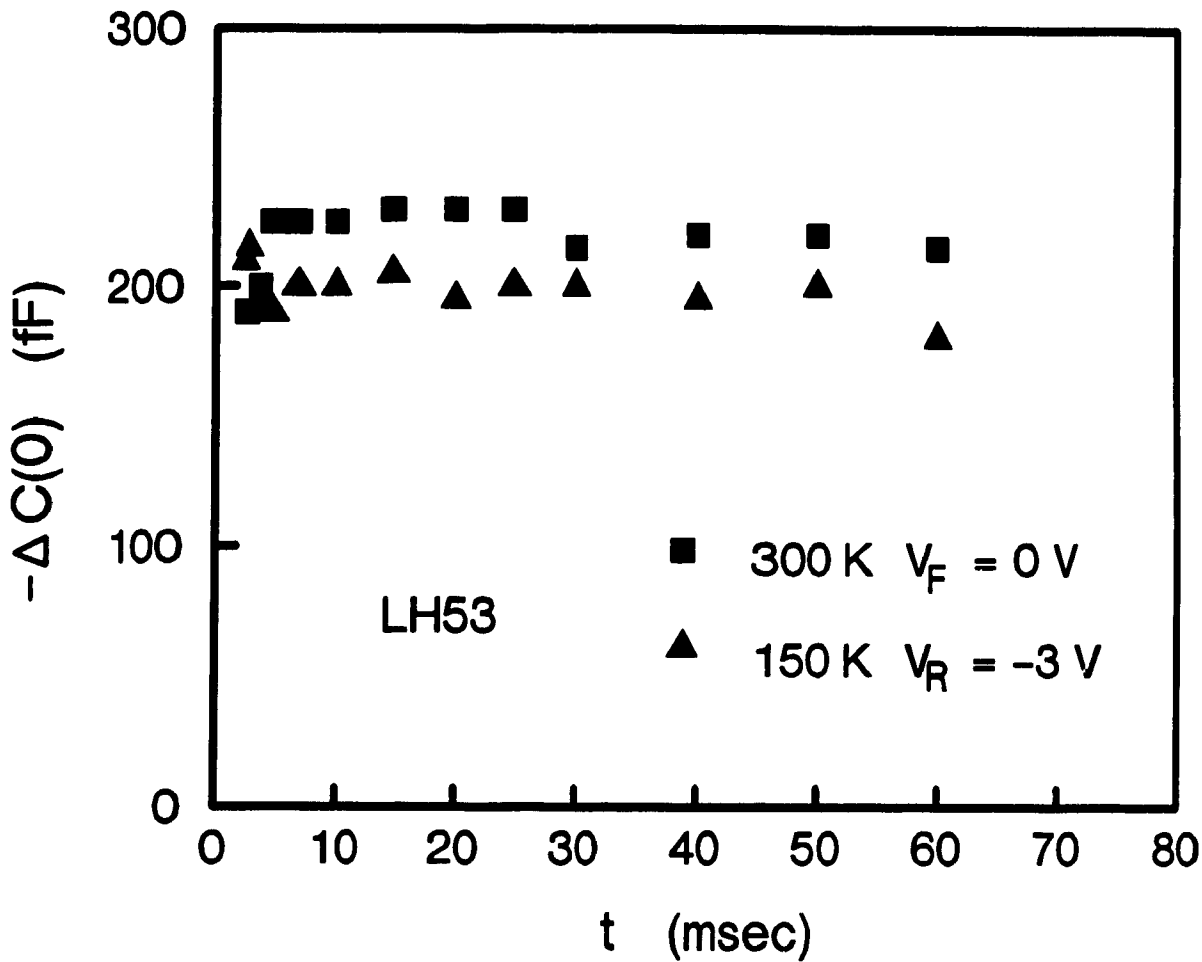


Fig.4.2 Plots of transient capacitance for hole traps with the majority carrier pulse duration showing the effect of the majority carrier pulse duration.

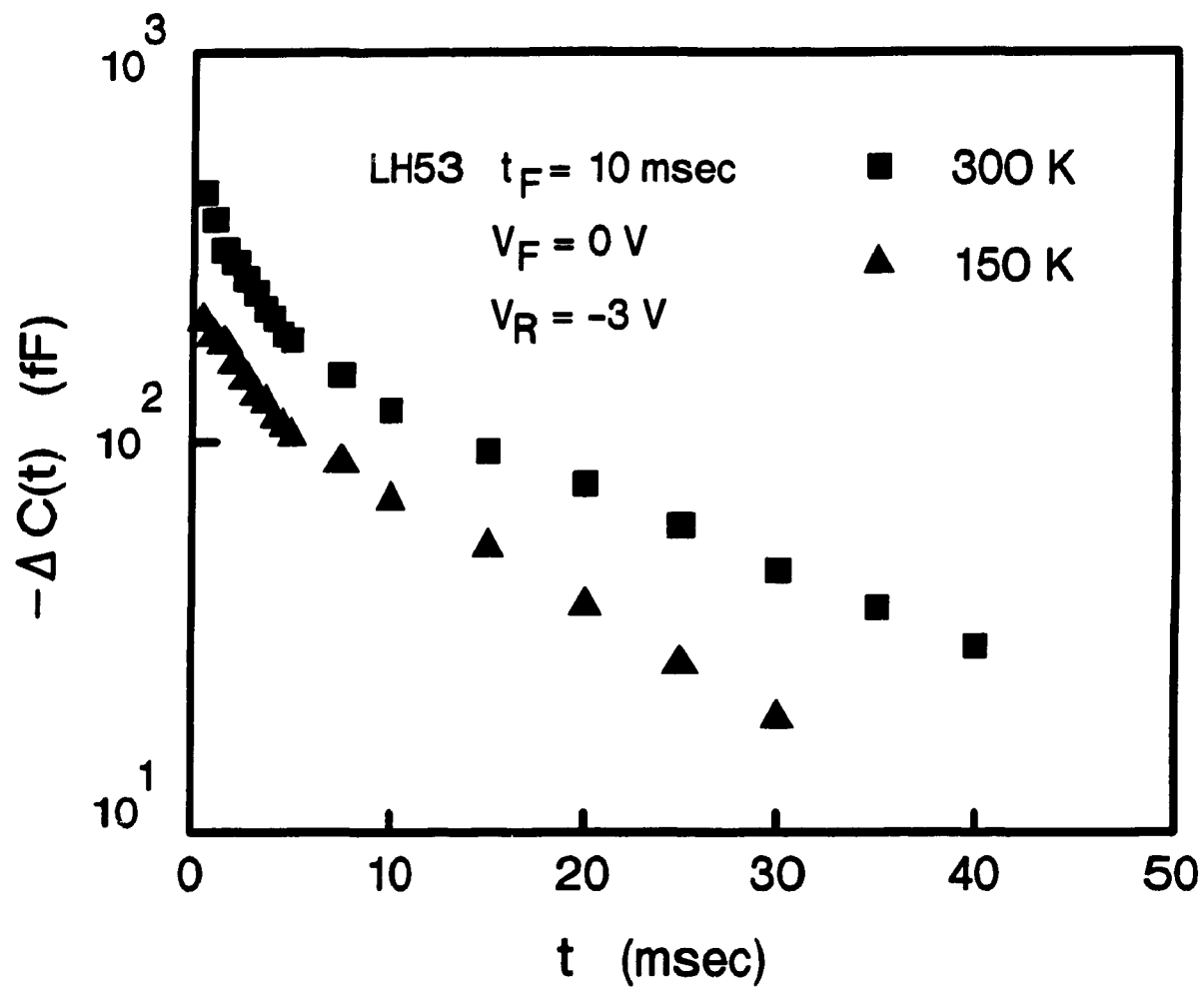


Fig.4.3 A semilog plot of transient capacitance with time for the sample LH53.

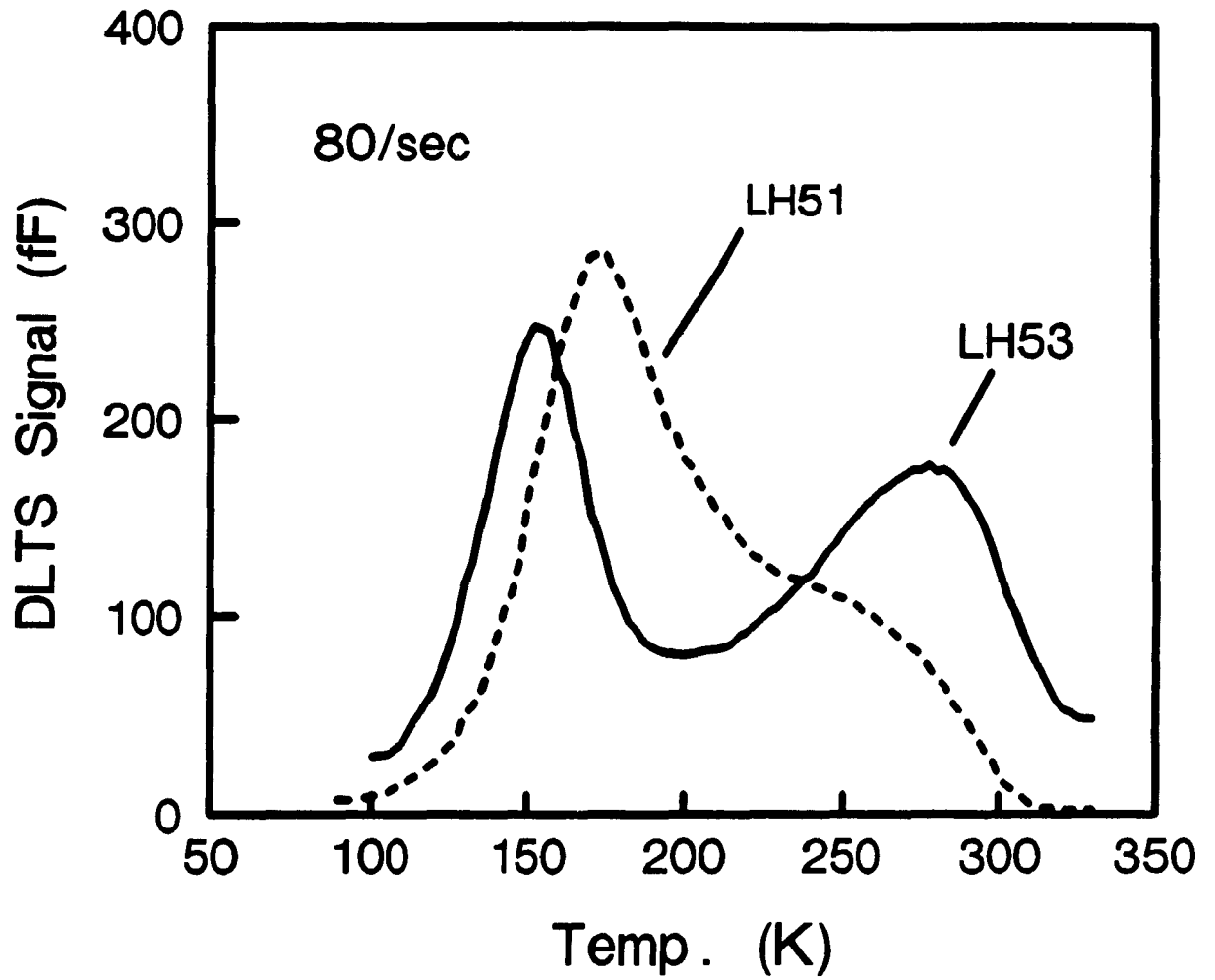


Fig.4.4 DLTS spectra of the samples LH51 and LH53 using a majority carrier pulse.

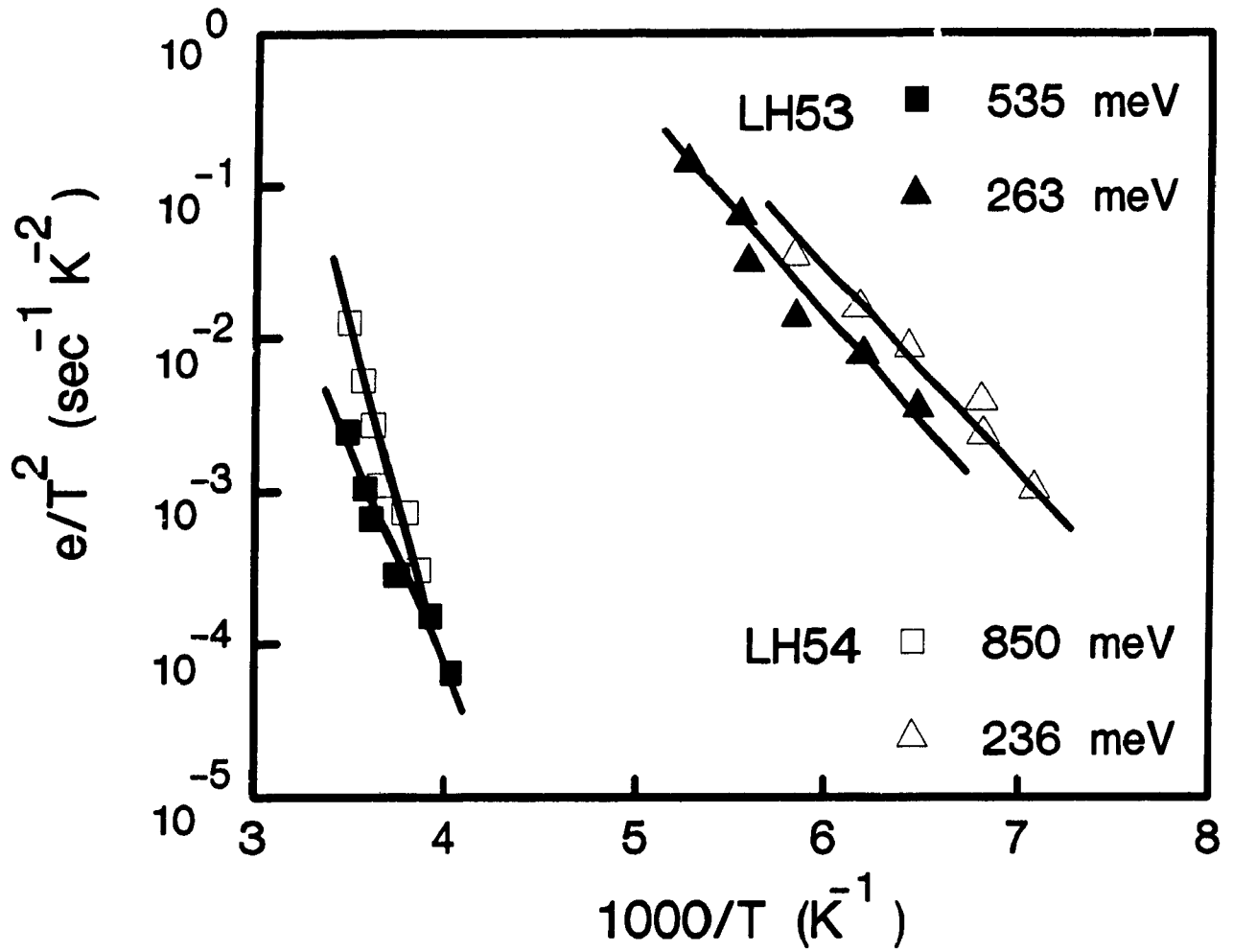


Fig.4.5 Arrhenius plots of the samples LH53 and LH54 of DLTS spectra with a majority carrier pulse (holes).

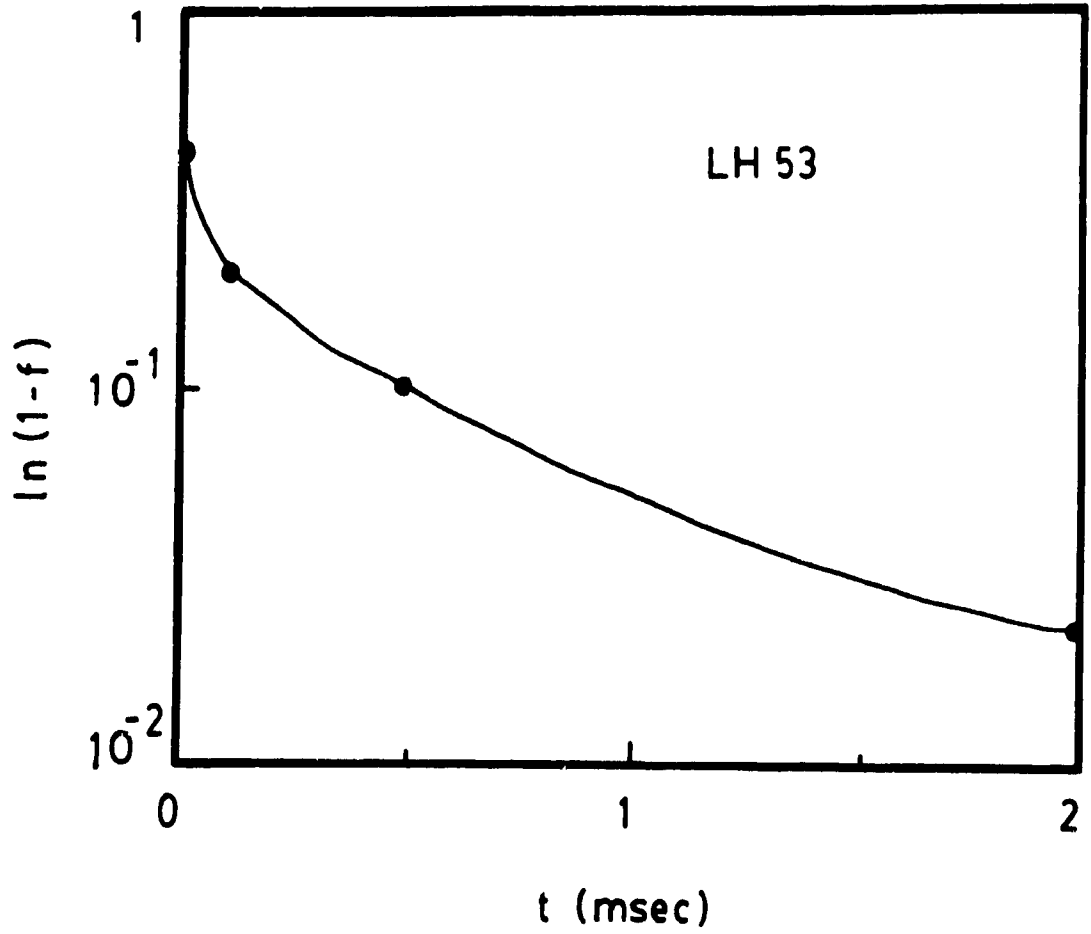


Fig.4.6 A plot of  $\ln(1-f)$  versus pulse duration  $t$ .

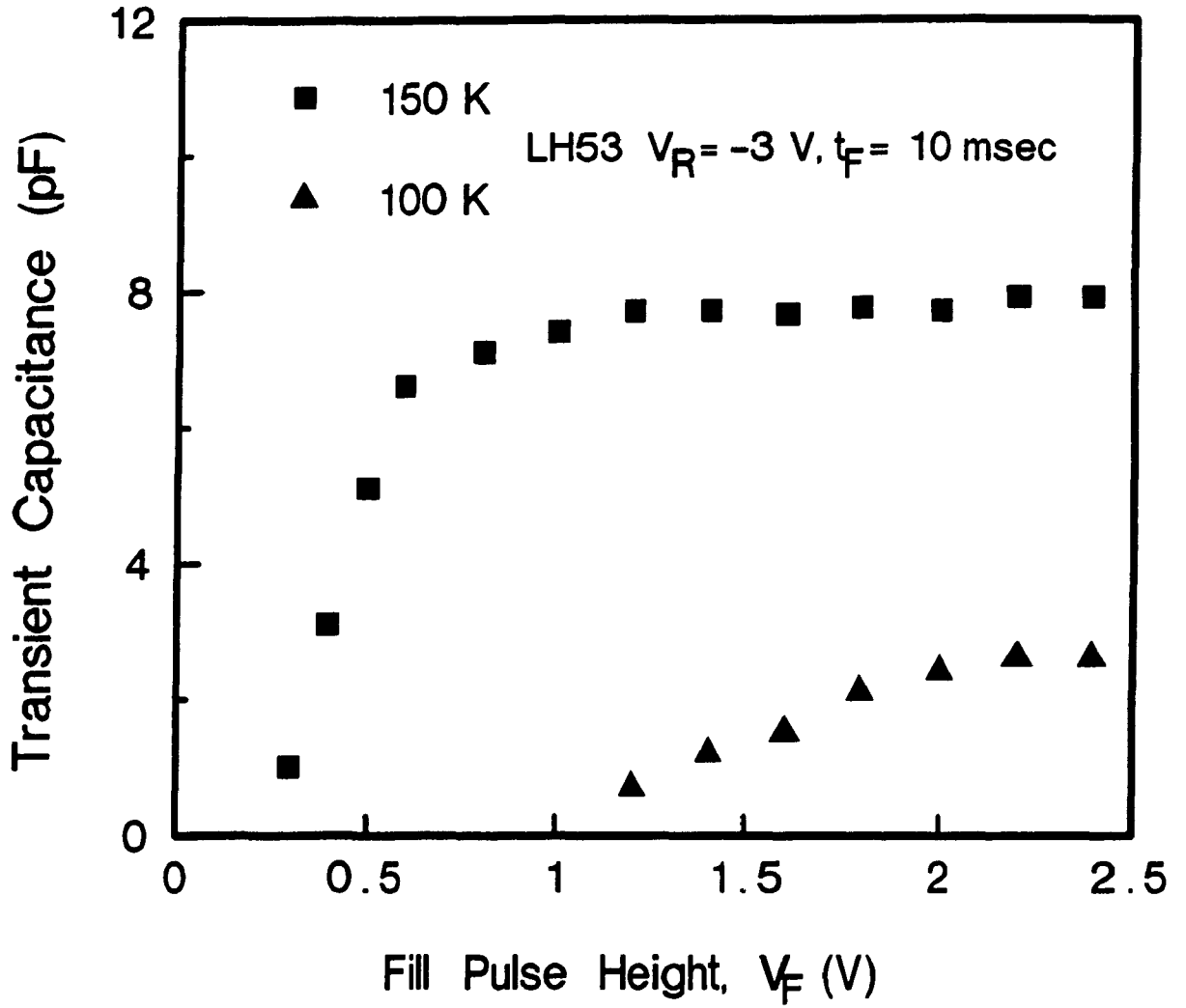


Fig.4.7 Dependence of capacitance transients on injection pulse height for the sample LH53.

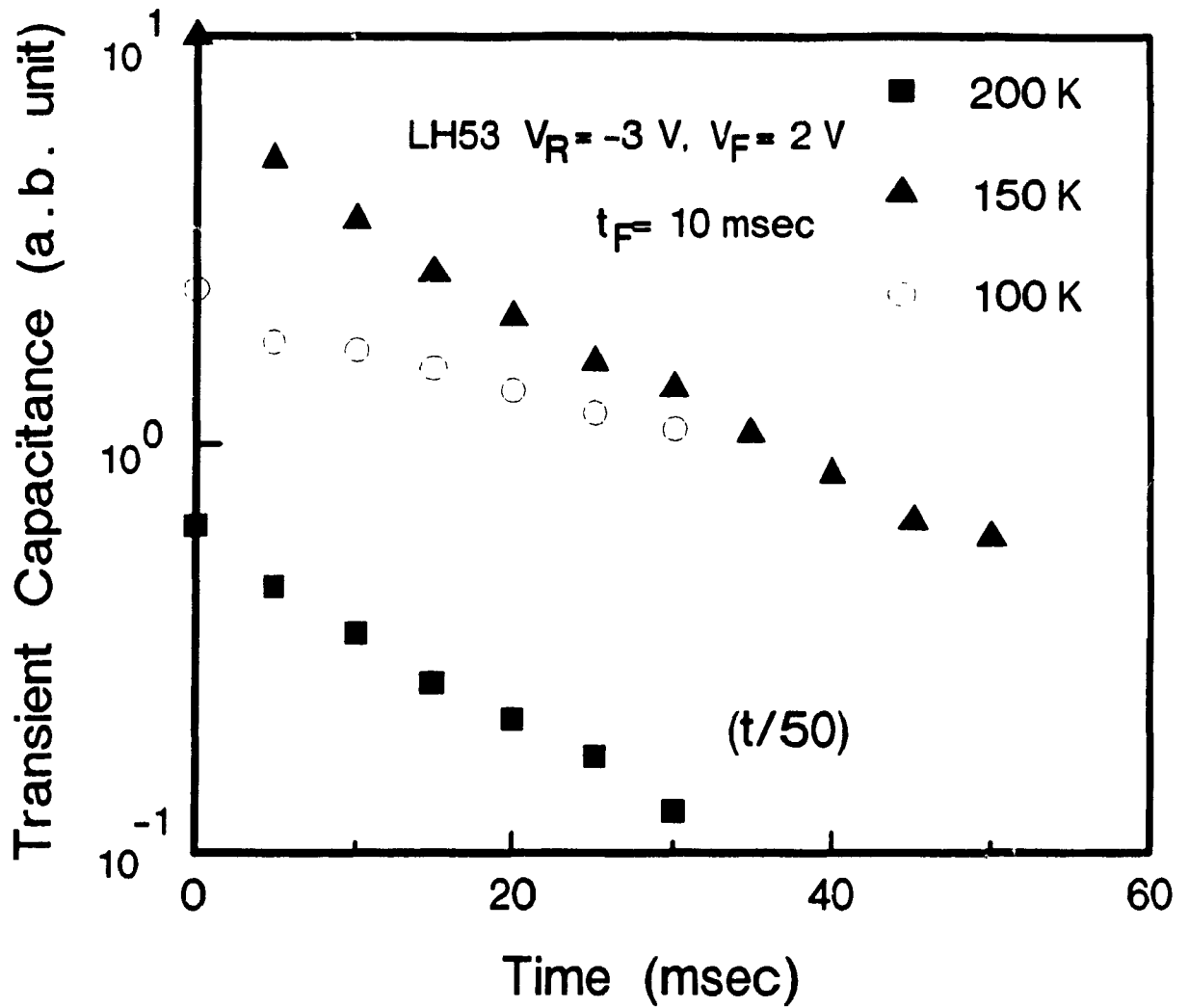


Fig.4.8 Semilog plots of capacitance transients with time at 100 K, 150 K and 200 K for the sample LH53.

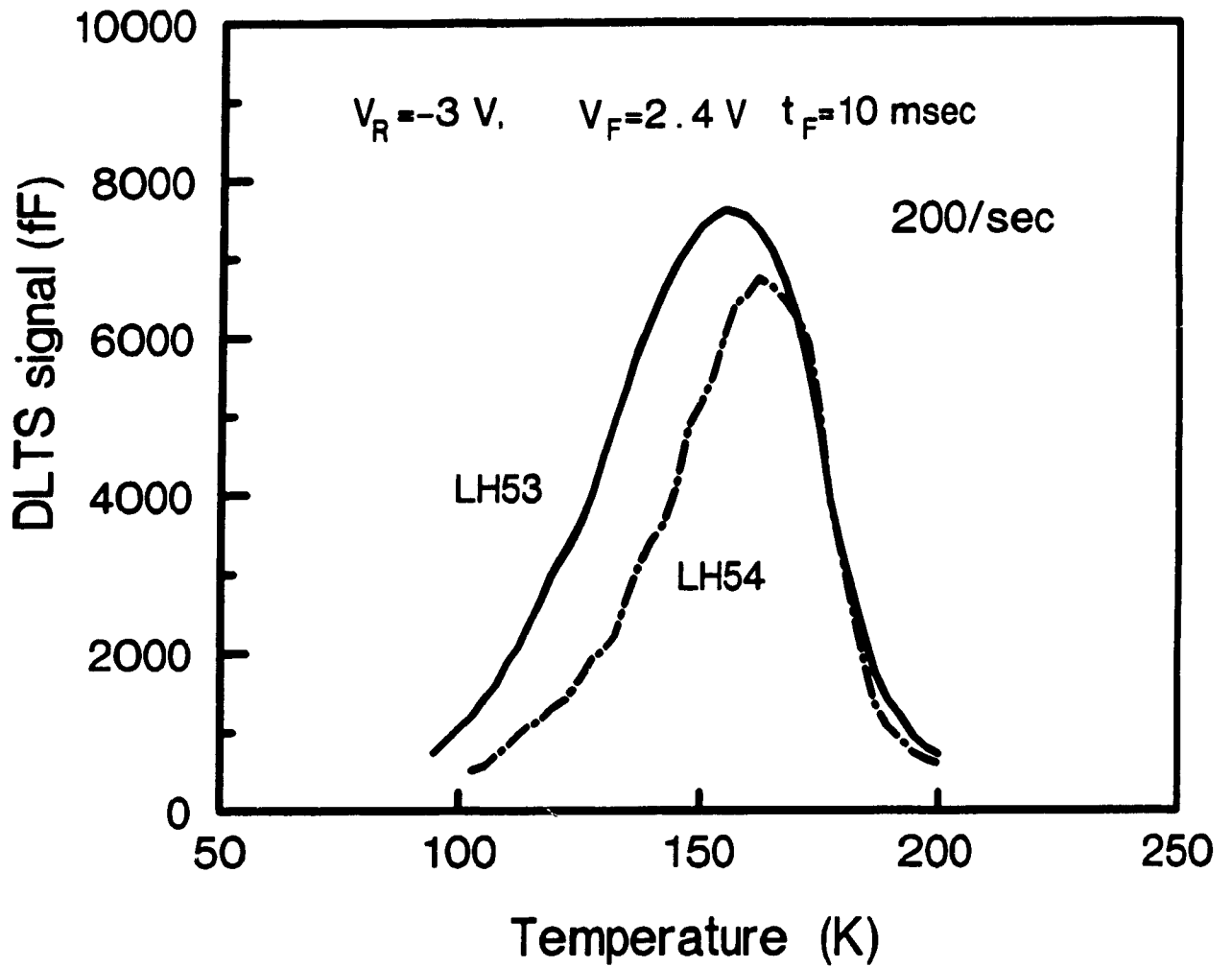


Fig.4.9 DLTS spectra of the samples LH53 and LH54 with an injection pulse.

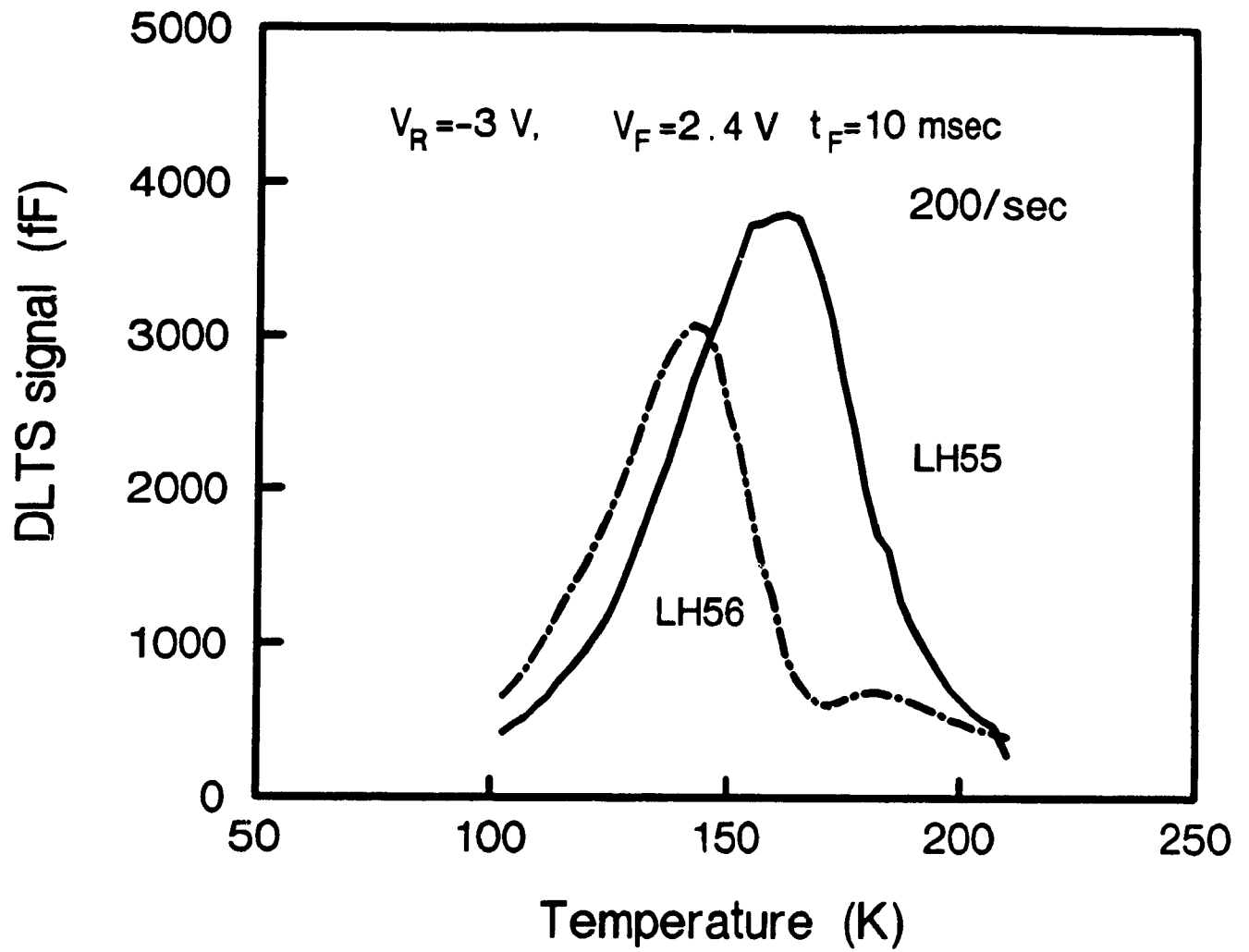


Fig.4.10 DLTS spectra of the samples LH55 and LH56 with an injection pulse.

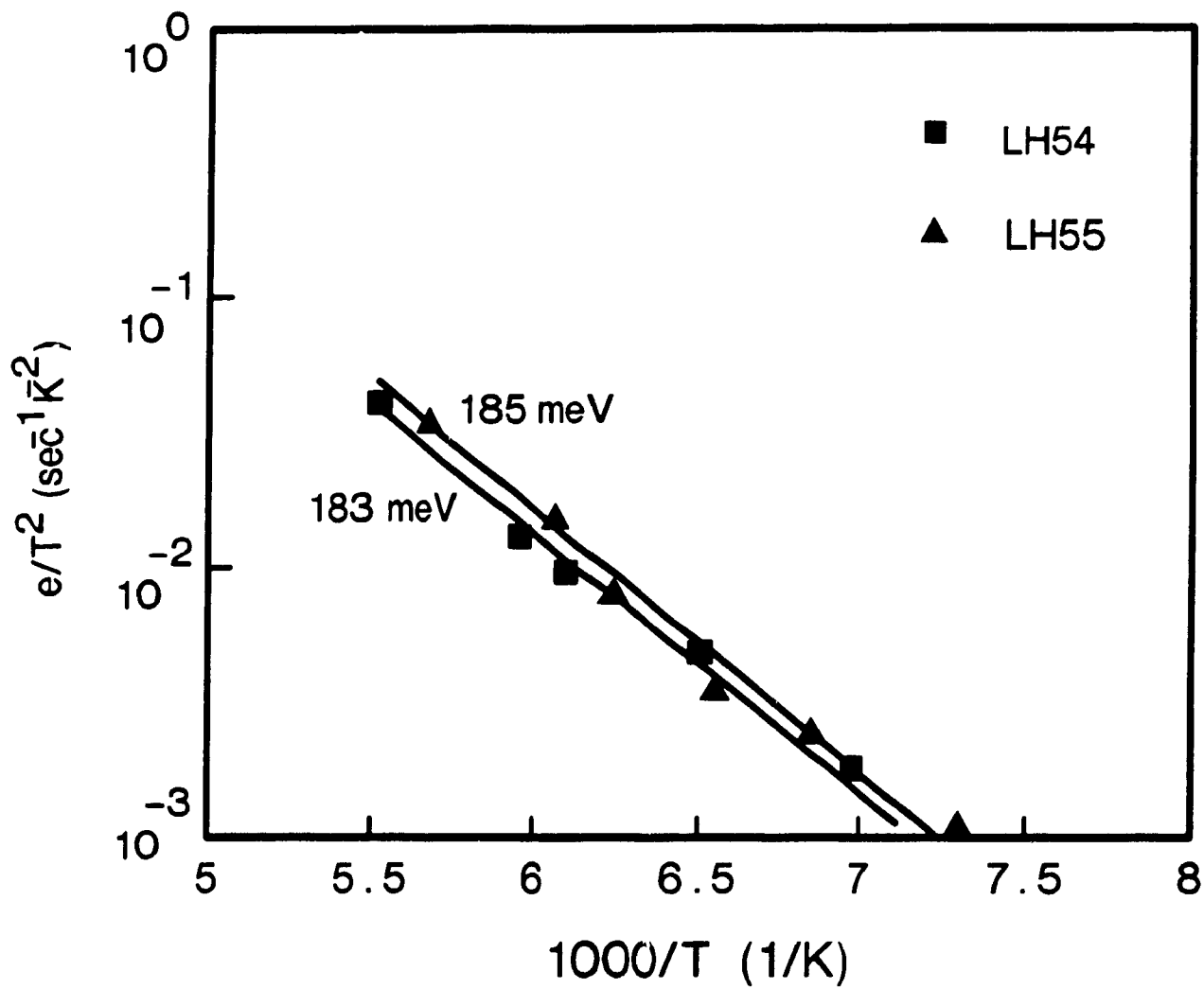


Fig.4.11 Arrhenius plots of the samples LH54 and LH55 for electron traps.

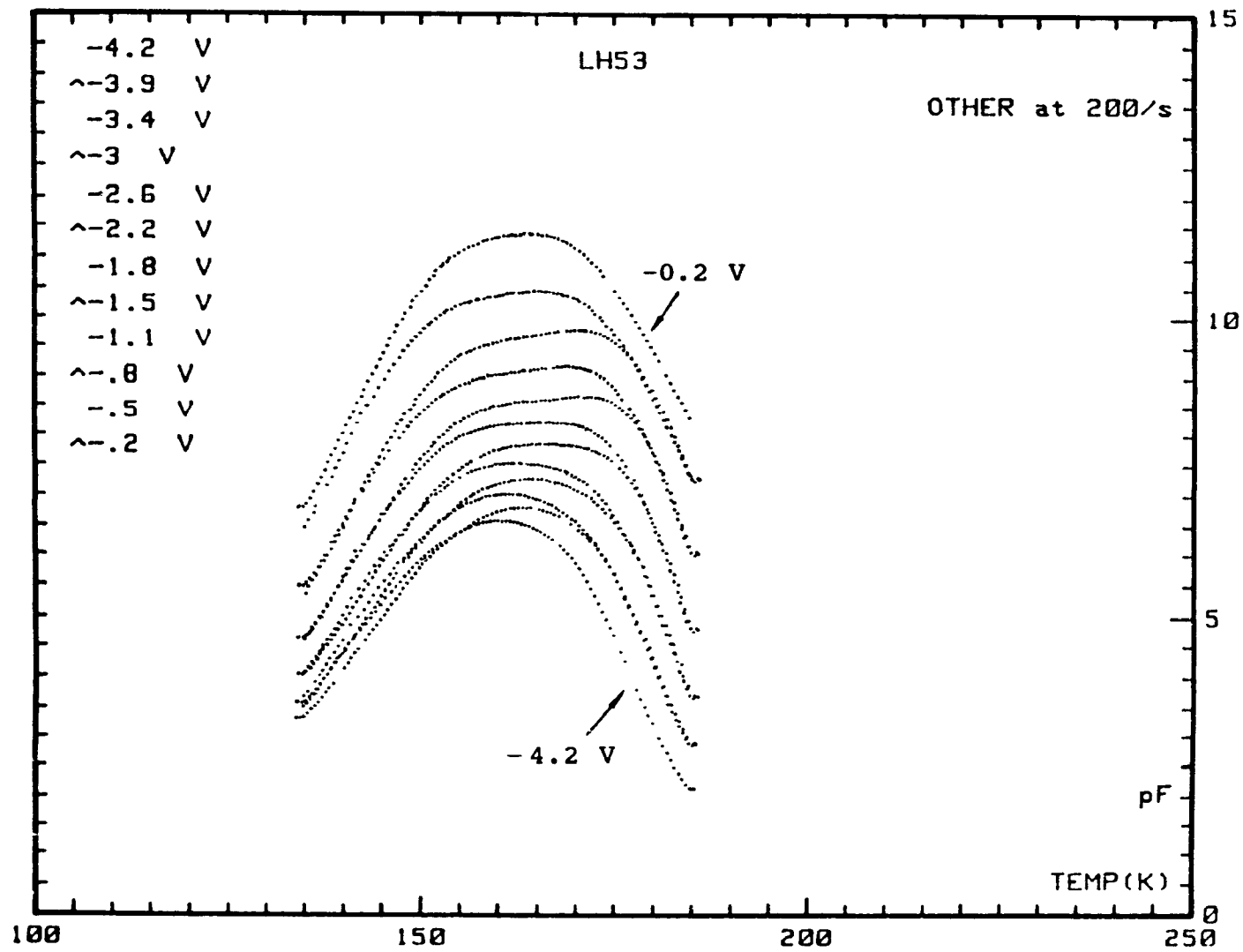


Fig.4.12 DLTS spectra of the sample LH53 at different reverse bias voltages.

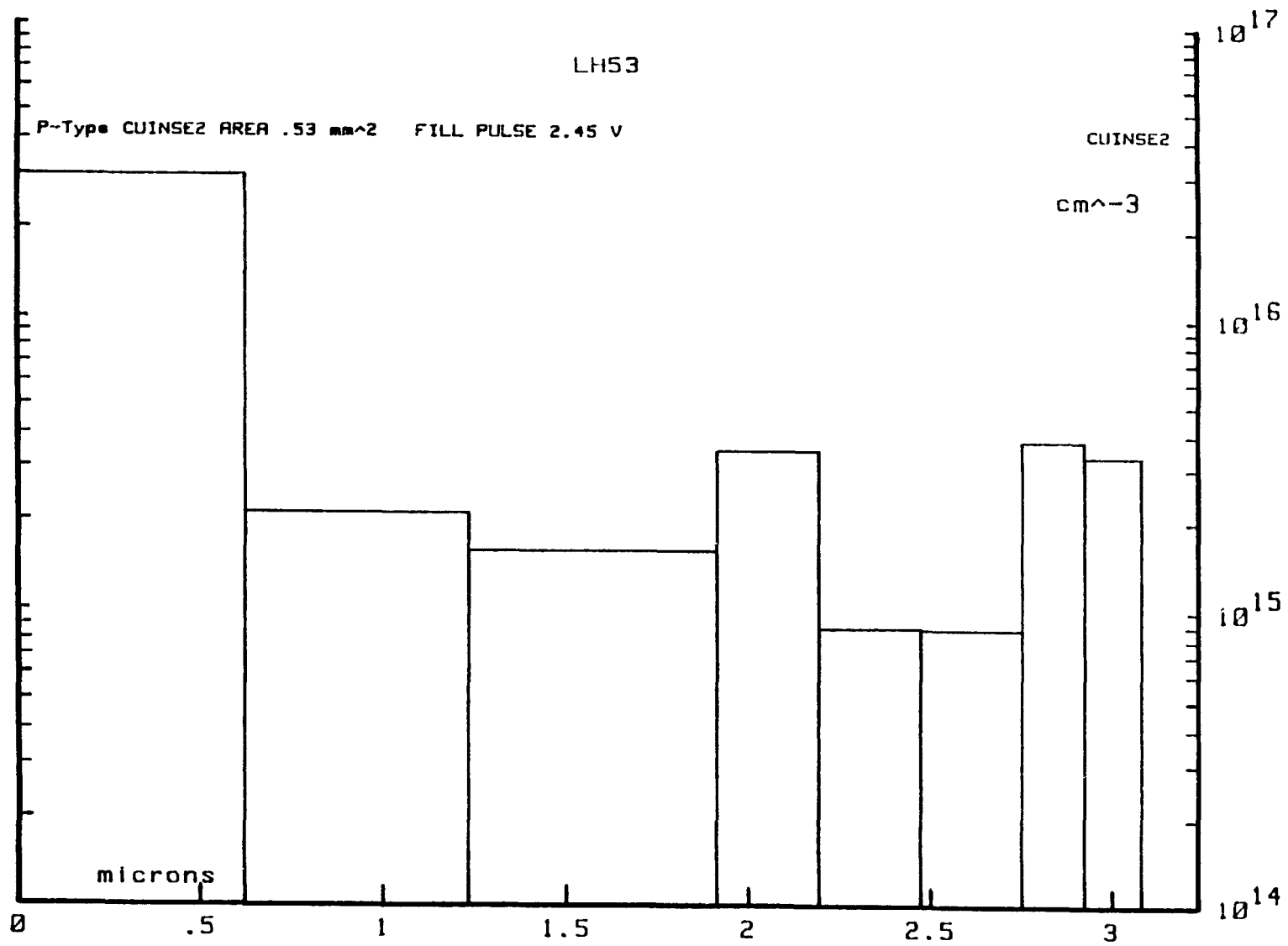


Fig.4.13 A plot of electron trap concentration with distance from the junction of the sample LH53 showing a large value near the interface.

## Chapter 5 Conclusions

Since the compound semiconductor  $\text{CuInSe}_2$  is one of the best candidate materials for solar cell applications, studies on defects of this material are very important. In the present work, homojunctions were fabricated by In or Bi diffusion into Bridgman-grown monocrystalline p-type  $\text{CuInSe}_2$  substrates. One of the advantages of using the homojunctions instead of heterojunctions is that the interface states and defects due to elemental interdiffusion can be minimized.

The current-voltage measurements have been carried out at different temperatures in order to understand the current transport mechanisms in this material. A model was used to analyze the I-V characteristics of these homojunctions. Accurate values of series resistance, shunt resistance, reverse saturation current and ideality factor were obtained by the computer fitting. From the results, it has been confirmed that the carrier recombination process is dominant in the current transport. The capacitance-voltage and capacitance-frequency measurements were also made on all of the samples. The acceptor densities in the p- $\text{CuInSe}_2$  of the homojunctions deduced from  $1/C^2$  versus  $V$  plots were about  $10^{15} \text{ cm}^{-3}$ . In addition, the

impurity concentrations in the regions near the surface were smaller than that far from the surface due to the compensation of acceptors by the diffused atoms. It was also found that the junction capacitance values at a fixed bias voltage decreased as the measuring frequency was increased. This effect suggested the existence of deep defects in the monocrystalline  $\text{CuInSe}_2$ .

In order to obtain quantitative data on the deep levels such as activation energies, trap densities and capture cross sections, both capacitance transient and DLTS measurements were performed on all of the samples. From results of the capacitance transients, it was found that only a single electron trap level and more than one hole trap level exist in the material. For the electron traps, the time constants of emission process were about 0.37 msec, 20 msec and 38 msec at 200 K, 150 K and 100 K respectively. The analysis of the capacitance transients at 300 K showed that the time constants of hole emission process were 2 msec and 20 msec by assuming two hole trap levels. The trap densities were calculated from either the capacitance transients or the DLTS spectra and the average value of electron trap densities was about  $6.4 \times 10^{14} \text{ cm}^{-3}$ . For the hole traps, the densities were in the order of  $10^{13} \text{ cm}^{-3}$ .

From the two peaks obtained in the DLTS measurements with majority carrier pulses (hole traps), Arrhenius plots were obtained. The Arrhenius plots showed that the first acceptor

level located at  $250 \pm 15$  meV and the second one at  $520 \pm 15$  meV from the valence band edge. The above energy levels were obtained from the samples which were treated at  $200^{\circ}\text{C}$  in  $\text{N}_2$ . For the sample treated in air, the activation energy of the second level was 850 meV. This fact suggested that O atoms may have created a new level or formed a new defect center with the original atoms associated with the defects.

The electron traps were investigated on the two kinds of samples treated in  $\text{N}_2$  or air by carrying out DLTS measurements with an injection pulse. The activation energy was  $182 \pm 14$  meV below the conduction band edge. It was also noted from DLTS spectra that the densities of electron traps in the samples formed by the Bi diffusion were smaller than that in the In-diffused junctions. Moreover, from the density profile, it was found that the apparent electron trap density near the sample surface was greater than that far from the surface. High concentration could be due to contamination during the diffusion process. The contamination seemed to be severe in the indium diffused junctions rather than the bismuth diffused ones. Alternatively, it is possible that the electron traps were introduced during the etching process or the cutting process, or the fixed doping concentration supplied to the computer for the calculation was not appropriate. To investigate the origin of the electron traps, more experiments will be needed.

The capture cross sections were obtained by either using the DLTS system or calculating from the intercept of the Arrhe-

nus plots. From the DLTS measurements with different pulse durations, it was found that the capture cross sections of the hole traps was from  $2.2 \times 10^{-19}$  to  $1.2 \times 10^{-18}$   $\text{cm}^2$ . The results suggested that the hole traps may have a broad energy distribution or there exist a non-flat energy bend at a small filling pulse during the measurements. Since it was difficult to determine the densities of the injected electrons, the electron trap capture cross sections were only calculated from the Arrhenius plots. The value for the sample treated at  $200^\circ\text{C}$  for 10 minutes in  $\text{N}_2$  was about  $1.58 \times 10^{-17}$   $\text{cm}^2$ . In order to obtain more information about the electron traps, the DLTS system with a laser excitation unit or devices fabricated using n-type  $\text{CuInSe}_2$  substrates should be used.

## References

- 1.1. S.M. Wasim, Solar Cells, Vol. 16, 1986, pp. 289.
- 1.2. K.J. Bachmann, M. Fearheiley, Y.H. Shing and N. Tran, Appl. Phys. Lett., Vol. 44, No. 4, 1984, pp. 407.
- 1.3. H. Haupt and K. Hess, Inst. Phys. Conf. Ser., No. 35, 1977, pp. 5.
- 1.4. T.F. Ciszek, J. Electron. Mater., Vol. 14, No. 4, 1985, pp. 451.
- 1.5. J. Parkes, R.D. Tomlinson and M.J. Hampshire, J. Cryst. Growth, Vol. 20, 1973, pp. 315.
- 1.6. I. Shih, C.H. Champness and A. Vahid Shahidi, Solar Cells, Vol. 16, 1986, pp. 27.
- 1.7. W.S. Weng, L.S. Yip, I. Shih and C.H. Champness, Can. J. Phys., Vol. 67, 1989, pp. 294.
- 1.8. M.G. Buehler, Solid-State Electron., Vol. 15, 1972, pp. 69.
- 1.9. D. Eirug Davies and S. Roosild, Appl. Phys. Lett., Vol. 18, 1971, pp. 548.
- 1.10. D.L. Losee, Appl. Phys. Lett., Vol. 4, No. 2, 1972, pp. 54.

- 1.11. R. Williams, J. Appl. Phys., Vol. 37, No. 9, 1966, pp. 3411.
- 1.12. D.V. Lang, J. Appl. Phys., Vol. 45, No. 7, 1974, pp. 3014.
- 1.13. C.T. Sah, W.W. Chan, H.S. Fu and J.W. Walker, Appl. Phys. Lett., Vol. 20, No. 5, 1972, pp. 193.
- 1.14. C.T. Sah and J.W. Walker, Appl. Phys. Lett., Vol. 22, No. 8, 1973, pp. 384.
- 1.15. C.T. Sah, L.L. Rosier and A.F. Tasch, Jr., Solid-State Electron., Vol. 13, pp. 759.
- 1.16. J.C. Carballes and J. Varon, Solid State Commun., Vol. 9, 1971, pp. 1627.
- 1.17. H. Kukimoto, C.H. Henry and F.R. Merritt, Phys. Rev. B, Vol. 7, No. 6, 1973, pp. 2486.
- 1.18. L.D. Yau and C.T. Sah, Phys. Stat. Sol. (a), Vol. 6, 1971, pp. 561.
- 1.19. C.H. Henry, H. Kukimoto, G.L. Miller and F.R. Merritt, Phys. Rev. B, Vol. 7, No. 5, 1973, pp. 2499.
- 1.20. D.V. Lang, J. Appl. Phys., Vol. 45, No. 7, 1974, pp. 3023.
- 1.21. Alew C. Wang and C.T. Sah, J. Appl. Phys., Vol. 57, 1985, pp. 4645.
- 1.22. N.M. Eron and A. Rothwarf, Proc. 17th IEEE Photovoltaic Spec. Conf., IEEE New York, 1984, pp. 876.

- 1.23. L.B. Fabik and K. Eskenas, Proc. 18th IEEE Photovoltaic Spec. Conf., IEEE New York, 1984, pp. 754.
- 1.24. R.K. Ahrenkiel, Solar Cells, Vol. 16, 1986, pp. 549.
- 1.25. T.R. Hanak, A.M. Bakry, D.J. Dunlavy, F. Abou-Elfotouh, R.K. Ahrenkiel and M.L. Timmons, Solar Cells, Vol. 27, 1989, pp. 347.
- 1.26. N. Christoforou and J.D. Leslie, Solar Cells, Vol. 26, 1989, pp. 197.
- 1.27. C.X. Qiu and I. Shih, Solar Cells, Vol. 16, 1986, pp. 391.
- 1.28. H. Neumann, N. Van Nam, H.J. Hobler and G. Kuhn, Solid State Commun., Vol. 25, 1978, pp. 899.
- 1.29. T. Irie, S. Endo and S. Kimura, Jpn. J. Appl. Phys., Vol. 18, 1979, pp. 1303.
- 1.30. H. Sobotta, H. Neumann, V. Riede, G. Kuhn, J. Seltmann and D. Opermann, Phys. Stat. Sol. (a), Vol. 60, 1980, pp. 531.
- 1.31. I. Shih and L. Li, Submitted to Journal of Applied Physics.
- 2.1. W. Shockley, Bell Syst. Tech. J., Vol. 28, 1949, pp. 435.
- 2.2. S.M. Sze, Physics of Semiconductor Devices (Second Edition), John Wiley and Sons, New York, 1981, pp. 19.
- 2.3. Wesley A. Miller and Larry C. Olsen, IEEE Trans. Electron Devices, Vol. ED-31, No. 5, 1984, pp. 654.

- 2.4. W.A. Miller, Proc. 17th IEEE Photovoltaic Spec. Conf., IEEE New York, 1984, pp. 768.
- 2.5. N. Christoforou, A Study of Deep Levels in  $\text{CuInSe}_2$  by Current-Voltage, Capacitance-Voltage, and Capacitance Transient Measurements on  $\text{CdS/CuInSe}_2$ , Ph.D thesis, University of Waterloo, 1987.
- 2.6. A.G. Milnes, Deep Impurities in Semiconductors, John Wiley and Sons, New York, 1973, pp. 193.
- 3.1. O. Engstrom and A. Alm, Solid-State Electron., Vol. 21, 1978, pp. 1571.
- 3.2. C.H. Henry, H. Kukimoto, G.L. Miller and F.R. Merritt, Phy. Rev., B, Vol. 7, 1973, pp. 2499.
- 3.3. D.V. Lang, J. Appl. Phys., Vol. 45, 1974, pp. 3014.
- 3.4. M.C. Chen, D.V. Lang, W.C. Dautremont-Smith, A.M. Sergent and J.P. Haribison, Appl. Phys. Lett., Vol. 44, 1984, pp. 790.
- 3.5. W.I. Lee and J.M. Borrego, J. Appl. Phys., Vol. 63, 1988, pp. 5357.
- 4.1. H.K. Kim, T.E. Schlesinger and A.G. Milnes, J. Electron. Mater., Vol. 17, 1988, pp. 187.